5

Interaction of Direct Current and Extremely Low-Frequency Electric Fields with Biological Materials and Systems

Frank S. Barnes

CONTENTS

5.1 Introduction

The fact that electrical currents can affect the behavior of biological systems has been known for more than 2000 years. Electric shocks have been used to treat a wide variety of ailments since the eighteenth century. However, our knowledge of how these fields and the resulting currents influence biological systems is surprisingly incomplete. Electrical signals are clearly important in the control of biological processes and in carrying information from one part of the body to another. Nerve cells propagate electrical signals from sensors of pressure, temperature, light, sound, etc., to the brain and return control signals to muscles and other tissue. Yet, if we choose to stimulate these processes with external electrical inputs, we have a relatively limited understanding of how a given electrical signal will affect various biological organs; what the safe limits of exposure are (particularly overextended periods of time); and how electrical signals are carried across cell membranes, are propagated along nerves, or affect growth processes and cell division.

The purpose of this review is to bring together some of the physical concepts that underlie the interaction between electric fields and biological materials with the objective of providing background for determining safe levels of exposure and new applications for the use of electricity in therapy. This is the first step in a long chain of events that lead from externally applied electric field forces to significant biological changes. An objective of this chapter is to provide a background for some of the other chapters that cover both possible health effects and some therapeutic applications of electric and magnetic fields.

The approach that will be taken is to start with Maxwell's equations and couple them to the bulk electric and magnetic properties of the materials. These equations allow us to calculate the values of the electric and magnetic fields as a function of time and space given the values for the dielectric constant and the conductivity. The techniques for the solution of these equations for a wide variety of biological systems are covered in Chapter 10 in this volume by J. Lin and P. Bemardi and for imaging see Chapter 12 in this volume by W.T. Joines, O.H. Liu and G. Ybarra. From the solutions of these equations for the electric and magnetic fields, the conservation of energy, and charge, expressions can be obtained for the current density and other parameters of interest.

Next, the force equations are used to develop equations for the conductivity and the dielectric constant. This section is organized to begin at the lowest level of complexity by examining some of the forces that are exerted on charged particles in fluids, and it then proceeds to some of the effects of electric fields on chemical reaction rates and membranes. At the next level of complexity, some effects of externally applied electric fields on currents through membranes and membrane nonlinearities are described. Some effects of high-level fields and electroporation are described in Chapter 9 in *BMA* by Weaver and Chizmadzhev [112]. This is followed by a discussion of some long-term adaptive processes and secondary effects of current flow due to heating and by a description of a few effects on whole animals. This information is presented with the objective of specifying the general level or intensity of fields, currents, and temperatures where one can expect to observe a given class of biological responses. Much more data are presented in Chapter 3 in *BMA* by Anderson et al. [113]. The next section contains data on the levels of typical naturally occurring and man-made fields. This section also includes a comparison of some externally applied fields, fundamental noise levels, and signals generated in the body. J. Weaver and M. Bier present a more complete treatment of some of the noise sources in biological cells in Chapter 7 in this volume.

5.2 Maxwell's Equations and the Properties of Materials

Maxwell's equations can be written in both differential and integral form, and solutions to them under a variety of boundary conditions are extensively covered in Chapter 10 in this volume by James C. Lin and Paolo Bernardi. In differential form they are given by [1]

$$\vec{\nabla} \times \vec{H} = \vec{J} + \frac{\partial \vec{d}}{\partial t} \tag{5.1}$$

$$\vec{\nabla} \times \vec{E} = -\frac{\partial \vec{B}}{\partial t} \tag{5.2}$$

$$\vec{d} = \varepsilon_0 \vec{E} + \vec{p} \tag{5.3}$$

$$\vec{B} = \mu_0 \vec{H} + \vec{M}_B \tag{5.4}$$

where $\vec{H}$ is the magnetic field, $\vec{J}$ is the current density, $\vec{d}$ is the displacement vector, t is time, $\vec{E}$ is the electric field, $\vec{\nabla}$ is the partial differential operator, del, $\vec{B}$ is the magnetic flux density, ε_0 is the dielectric constant for free space, $\vec{p}$ is the electrical polarization per unit volume, μ_0 is the magnetic permeability in vacuum, and $\vec{M}_B$ is the magnetic polarization per unit volume. It is often convenient to expand the electrical polarization in a power series:

$$\vec{p} = \vec{p}_0 + \varepsilon_0 X_e \vec{E} + \varepsilon_0 X_2 \vec{E}^2 + \cdots \tag{5.5}$$

where $\vec{p}_0$ is the permanent polarization, X_e is the linear electric susceptibility, and X_2 is the quadratic coefficient. X_2 is significant for nonlinear optics and very large values of the electric field. For most of the exposure conditions described in this volume it is convenient to express the induced polarization in terms of the dielectric constant ε

$$\varepsilon = \varepsilon_0 (1 + X_e) \tag{5.6}$$

Note that in anisotropic materials, both ε and X_e may be tensors and complex numbers. The imaginary part of ε is associated with the loss or dissipation of energy by the bound charges. The solutions to Maxwell's equations for $\vec{E}$ and $\vec{B}$ are given for a variety of boundary conditions and under the assumption that values for $\vec{J}$, $\vec{p}$, and $\vec{M}_B$ are known (given in Chapter 10 in this volume by James C. Lin and Paolo Bernardi). These fields, in turn, determine the forces on the components of the biological material.

5.3 Physics of the Interactions of Electric Fields with Biological Materials

Biological systems consist of complex physical subsystems. In an attempt to understand them, we will start at the most elementary level. Perhaps the simplest level—which is already surprisingly complicated—is the effect of electric fields on biological fluids. These fluids contain a large number of components, including ions, polar molecules such as water, proteins, lipids, hormones, and colloidal particles. Current flow in these fluids is given by the sum of the drift and diffusion currents for each component. At low current densities the system is linear; however, at moderate to high current densities nonlinearities are observed [2]. In addition, the fields can change the orientation of molecules with dipole moments, induce dipoles by distorting electron orbits, and change the relative positions of some of the atoms within the molecule. This, in turn, leads to changes in the dielectric constant. The next level of complexity involves the interaction of the fields with membranes that behave like porous solids for fields applied perpendicularly to their surface and like viscous liquids for fields in the plane of the membrane [3,4]. Membranes are inhomogenous so that different portions of them may be affected differently by the perturbing fields. Additionally, membranes are involved in active chemical reactions that change their porosity to various ions selectively. Both electrical potentials and chemical signals may change the membranes' conductivity by orders of magnitude and transmit signals across membranes. The next level of complexity occurs in the interactions between

the biological fluids and the membranes in the presence of electric fields. Electric fields affect the selective transport of ions or molecules through the membrane. They change the buildup of charged ion layers at the surface and change the way new molecules are incorporated into the membrane or are bound to its surface. The result of changes in the transport of molecules or ions across cell membranes is changes in the performance of the cells and, in turn, of the organs of which they are a part. They can also lead to changes in the rate of exchange of electrons between molecules in the membrane and ions or molecules in the fluid [5]. For example, a biasing electric voltage across a pacemaker cell in the heart will change its firing rate and thus the pumping rate of the heart.

The fundamental law describing the forces on charged particles is given by

$$\vec{F} = q(\vec{E} + \vec{v} \times \vec{B}) \tag{5.7}$$

where $\vec{F}$ is the force, q is the charge on the particle, and $\vec{v}$ is the velocity of the particle. $\vec{E}$ and $\vec{B}$ are coupled by Maxwell's equations so that a time-varying magnetic field generates an $\vec{E}$ field and vice versa. This force may lead to ion currents and changes in the orientation of dipoles in molecules, and it may also lead to transitions between energy levels, to shifts in their spacing and induced dipole moments, $\vec{P}$. Additionally, if nonlinearities or time-varying impedances are present, alternating current (AC) fields can be rectified to produce direct current (DC), frequencies at the second and higher harmonics, and sum and difference frequencies with biological or molecular oscillations. Direct magnetic field effects may occur through the term $\vec{v} \times \vec{B}$. For example, for a Na^+ moving at a thermal velocity of 4×10^2 m/sec in the earth's magnetic field of about 5×10^{-5} T, this term has a magnitude of 2×10^{-2} V/m, and the force is at right angles to the field and the velocity.

In addition to the forces on charged particles, electric fields can induce forces on polarizable atoms, molecules, ions, and molecules with dipole moments. To first order these forces are described by

$$\vec{F}_{\mathrm{d}} = (\vec{P}_0 \cdot \vec{\nabla})\vec{E} \tag{5.8}$$

$$\vec{F}_{\mathrm{L}} = \boldsymbol{\alpha} V(\vec{E} \cdot \vec{\nabla})\vec{E} \tag{5.9}$$

where $\vec{F}_{\mathrm{d}}$ is the force on a molecule with a permanent dipole moment $\vec{P}_0$, and $\vec{\nabla}\vec{E}$ is the gradient of the electric field. $\vec{F}_{\mathrm{L}}$ is the force on a molecule with an induced dipole moment $\vec{P}_{\mathrm{i}} = \boldsymbol{\alpha} V\vec{E}$, where α is the tensor polarizability and V is the volume [6]. Note that biological materials are highly inhomogenous and that there are large electric field gradients at the boundaries between the fluids and membranes. Additionally, for induced dipole moments, when the sign of the dipole reverses with an alternating field the force along the gradient of the field can be in a constant direction.

The current flow $\vec{J}_{\mathrm{i}}$ of a given molecule or ion, in molecules or ions per second per meter square, has both drift and diffusion components that may be given by

$$\vec{J}_{\mathrm{i}} = N_{\mathrm{i}}\mu\vec{F} + qD\vec{\nabla}N_{\mathrm{i}} \tag{5.10}$$

where N_{i} is the ion concentration, μ is the mobility in seconds per kilogram, D is the diffusion constant in meter square per second, and $\vec{\nabla}N_{\mathrm{i}}$ is the gradient of the concentration. For charged particles, the force has two components [7]:

$$\vec{F} = q\vec{E} + (\vec{M} \cdot \vec{\nabla}\vec{E}) \tag{5.11}$$

where $\vec{M}$ is the sum of the permanent and induced dipole moments.

The drift portion of the ion currents takes the form

$$\vec{J} = \sum q_i N_i \mu_i \vec{E} + \sum N_i \mu_i (\vec{M} \cdot \vec{\nabla}) \vec{E} \tag{5.12}$$

The conductivity $\sigma = \sum q_i N_i \mu_i$, and N_i is the concentration of each ion, μ_i is the mobility, and $\vec{M}_i$ is the dipole moment. Table 5.1 shows some typical values of mobility.

The conductivity of biological fluids such as blood, which contains cells, is in the vicinity of $\sigma = 0.6\,\mathrm{S/m}$, while for physiological saline it is approximately $1.4\,\mathrm{S/m}$. For more detailed material on the conductivities and dielectric constants of biological materials, see Chapter 3 in this volume by C. Gabriel. If the fluid channels between cells are relatively thick and the fluids are relatively good conductors, the channels tend to short circuit the voltages that might otherwise appear across membranes that typically have conductivities at least a thousand times smaller.

The total dielectric constant for a material includes the sum of the induced polarizabilities of the components and interaction terms between them. It is sometimes useful to think of the dielectric constant as a way of describing the fraction of the electric field that is shorted out by the bound charges. This can be shown by considering an ideal parallel plate capacitor where the outside plates are separated by a distance l. The capacity for these plates is given by

$$C_0 = \frac{\varepsilon_0 A}{l} \tag{5.13}$$

If an ideal thin metal plate of thickness w is inserted halfway between these plates, then the resulting capacity is given by

$$C = \frac{C_0}{(1 - w/l)} = \frac{\varepsilon A}{l} \tag{5.14}$$

The corresponding dielectric constant is given by

$$\varepsilon = \frac{\varepsilon_0}{(1 - w/l)} \tag{5.15}$$

In this example it is apparent that as the fraction of the field that is shorted out by the metal plate of thickness w increases, so does the effective dielectric constant. The electrons or ions forming an induced dipole moment can be thought of as doing the same thing. If there is a significant time lag for the movement of the charge, the effective value of w is reduced. The very large values of the dielectric constants of some tissues at low-frequencies can be thought of as the resulting motion of ions that are trapped inside highly

TABLE 5.1

Typical Values of Biological Ionic Mobilities

Particles	Mobilities	Ions	Mobilities
Proteins	$\mu = 10^{-10}$ to $10^{-8}\ \mathrm{m^2/V\,sec}$	Ca^{2+}	$\mu = 6.2 \times 10^{-8}\ \mathrm{m^2/V\,sec}$
Na^+	$\mu = 5.2 \times 10^{-8}\ \mathrm{m^2/V\,sec}$	Mg^+	$\mu = 5.4 \times 10^{-8}\ \mathrm{m^2/V\,sec}$
K^+	$\mu = 7.6 \times 10^{-8}\ \mathrm{m^2/V\,sec}$	Cr^+	$\mu = 1.9 \times 10^{-8}\ \mathrm{m^2/V\,sec}$

resistive membranes. At higher frequencies, the ions can no longer move fast enough to fully charge the surfaces of the membranes, and the effective dielectric constant for the tissue decreases. If energy is absorbed in inducing the dipole moments, then the dielectric constant becomes a complex number.

The forces applied by an electric field superimpose a drift velocity on the much larger random thermal velocity in the opposite directions for positively and negatively charged particles. These forces can lead to a redistribution of ions or molecules as a result of the differential mobilities and to an increase in the concentration of ions at interfaces. The average drift velocity $\vec{v}$ for a charged particle is given by

$$\vec{v} = \mu_i \vec{E} \tag{5.16}$$

The separation of molecules as a result of the different velocities in a DC electric field is known as electrophoresis and is frequently used to identify large molecules or charged colloidal particles [8]. The separation of particles in an AC field gradient is known as dielectrophoresis [5].

For a spherical particle in a homogenous insulating fluid the mobility μ_i is given by

$$\mu_i = q/6\pi\eta a \tag{5.17}$$

provided that the particle is significantly larger than the background particles of the fluid, where η is the viscosity of the fluid and a is the radius of the particle. In a conducting medium, counterions, or ions with a charge opposite to that of the particle, and molecules with dipole moments are attracted to it. They change the effective radius of the particle and then partially shield its charge. Additionally, small counterions may flow in the direction opposite to the particle motion, exerting a viscous drag. The theory for motion of a rigid sphere through a conducting liquid is complicated if all these effects are taken into account. Often some of the parameters, including the charge on the sphere, are not measurable. However, a relatively simple expression for the electrophoretic mobility is often used:

$$\mu_i = \frac{\varepsilon_i \zeta}{4\pi\eta} \tag{5.18}$$

where ε_i and η are the dielectric permittivity and the viscosity of the fluid (in kg/m sec), respectively, and ζ is the electrical potential drop from the particle surface across the bound fluid to the interface where the liquid begins to flow under the shear stress. Stated another way the ''zeta potential,'' ζ, is the potential at the surface boundary between the stationary fluid and the liquid that is moving with the particle. It should be noted that ζ is less than the total potential ψ across the charge double layer surrounding the charged particle. Also, note that water molecules bind to the ions, increase the effective diameter, and reduce the effective charge. This, in turn, makes the mobility less than that which might be expected at first from the atomic size and Stokes' law.

In a uniform AC field a charged particle oscillates about its mean position, and the electrical energy added to the solution is largely converted to heat. If there is a gradient in the field, as is to be expected in biological materials that are highly inhomogenous, then the gradient of the field can lead to a net charge displacement if the fields are large enough to lead to nonlinearities in the mobility or induced dipole moments. For large $\vec{E}$ the velocity saturates and mobility varies as

$$\mu_i = \frac{\mu_0'}{\left|\vec{E}\right|} \tag{5.19}$$

and Equation 5.16 yields

$$|\vec{v}| = \mu_0'$$

Most biological systems are highly inhomogenous, and the induced currents will vary rapidly in space. For the case of an induced dipole moment and an ideal dielectric sphere with a permittivity ε_2 and a conductivity $\sigma_2 = 0$ in an ideal dielectric fluid with a dielectric permittivity ε_1 and a conductivity $\sigma_1 = 0$ and a nonuniform electric field prior to inserting the sphere, the force

$$\vec{F}_{\mathbf{L}} = \boldsymbol{\alpha} V(\vec{E} \cdot \vec{\nabla})\vec{E} = 4\pi a^2 \varepsilon_1 \left\{ \frac{\varepsilon_2 - \varepsilon_1}{\varepsilon_2 + 2\varepsilon_1} \right\} \{(\vec{E}_1 \cdot \vec{\nabla})\vec{E}_1\} \tag{5.20}$$

where $\vec{E}_1$ is the field in the fluid prior to insertion of the sphere. Written another way

$$\vec{F}_{\mathrm{L}} = (3/2)V\varepsilon_1 \left\{ \frac{\varepsilon_2 - \varepsilon_1}{\varepsilon_2 + 2\varepsilon_1} \right\} \vec{\nabla} \left| \vec{E}_1 \right|^2 \tag{5.21}$$

If we assume that the viscous drag on a spherical particle is given by Stokes' law, then

$$\vec{F}_{\mathrm{d}} = 6\pi a \eta \vec{v} \tag{5.22}$$

and the mobility μ_{i} is given by

$$\mu_{\mathrm{i}} = (2a^2/3\eta)\varepsilon_1 \left\{ \frac{\varepsilon_2 - \varepsilon_1}{\varepsilon_2 + 2\varepsilon_1} \right\} \vec{\nabla}\vec{E}_1 \tag{5.23}$$

Dielectrophoresis may also be used for identifying molecules, and a more general treatment of the forces needs to take into account the conductivity or a complex dielectric constant for both the fluid and the particle [9].

For particles with dipole moments to change their distribution under the influence of an electric field gradient the force $\vec{F}$ must be large enough to overcome other forces. One of these forces that frequently must be overcome is due to osmotic pressure or diffusion. The osmotic pressure can be thought of as the force per unit area arising from diffusion or the random motion of the particles and is given by

$$\Pi = N_{\mathrm{i}} kT \tag{5.24}$$

where k is Boltzmann's constant and T is the absolute temperature [10]. The average differential force on a particle is proportional to the gradient of the osmotic pressure and is given by

$$\vec{F}_{\mathrm{os}} = -\frac{1}{N_{\mathrm{i}}} \vec{\nabla}\Pi = \frac{kT\vec{\nabla}N_{\mathrm{i}}}{N_{\mathrm{i}} - k\vec{\nabla}T} \tag{5.25}$$

If we consider the case of a spherical volume with a radial concentration gradient at constant temperature, the force is given by

$$\vec{F}_{\mathrm{os}} = -kT \frac{\Delta N_{\mathrm{i}}}{N_{\mathrm{i}}} \cdot \frac{r_0}{\Delta r} \tag{5.26}$$

where r_0 is the unit vector, ΔN_i is the incremental change in concentration, and Δr is the incremental change in distance. The maximum change is given by

$$\frac{\Delta N_i}{N_i} = 1 \tag{5.27}$$

when the presence or absence of a particle occurs at a distance $\Delta r = 2a$, where a is the particle radius. In this case, we get the maximum force

$$\left|\vec{F}_{os(max)}\right| = -\frac{kT}{2a} \tag{5.28}$$

To get an idea of the size of these forces, consider a particle of fat with $a = 1\,\mu m$ in water. The maximum osmotic pressure at $T = 300\,K$ is $|\vec{F}_{os(max)}| = 2 \times 10^{-13}\,N$. The dielectric constant for water is approximately $\varepsilon_1 = 80\varepsilon_0$ and for a fat particle, $\varepsilon_2 = 2\varepsilon_0$, where $\varepsilon_0 = 8.854 \times 10^{-12}\,F/m$. To get a dielectric force greater than the maximum osmotic force, we need a value of $\vec{\nabla} \mid \vec{E}_1 \mid^2 > 10^{12}\,V^2/m^3$. This is given approximately by a voltage of 100 V across a 5 mm gap when the $\vec{E}$ field goes from zero to a peak value of $5 \times 10^4\,V/m$ over the same gap. For a particle with a single charge in a uniform field, we would need a field of $E = 1.3 \times 10^4\,V/m$ to get an equal force.

The electric current densities generated by a concentration gradient are given by

$$\vec{J}_d = -qD\vec{\nabla}N_i \tag{5.29}$$

where D is the diffusion constant and is given by

$$D = \upsilon kT \tag{5.30}$$

where $\boldsymbol{\upsilon}$ is the hydrodynamic mobility with the dimensions of velocity/force and D has the dimensions of meter square per second. For rigid spherical particles of radius a, where $a \gg a_{H_2O}$, the Einstein–Stokes equation gives

$$D = \frac{kT}{6\pi\eta a} \tag{5.31}$$

This is only a first-order approximation because D varies slightly with concentration, departure of the molecule from a spherical shape, and other factors. η is the viscosity (in kg/m sec).

It is sometimes of interest to estimate the ratio of the drift to the diffusion current in order to estimate the level of the applied fields or the applied field gradients that lead to biological changes. This ratio is approximately given by [6]

$$\frac{\vec{J}_{i,diffusion}}{\vec{J}_{i,drift}} = \left(\frac{kT}{F_i}\right)\cdot\left(\frac{\Delta N_i}{N_i}\right) \tag{5.32}$$

where $\vec{F}_i$ is the force on the particle due to both the charge on the particle and the gradient of the field on the dipole moment. If we now assume that the maximum change in N_i goes from N_i in the solution to 0 at the membrane surface over a distance of the diameter of the

molecule of N_i and that this is the same distance over which the field goes from the field in the fluid to the field in the membrane, then

$$\frac{\vec{J}_{i,\text{diffusion}}}{\vec{J}_{i,\text{drift}}} = \frac{kT}{W_i} \tag{5.33}$$

where W_i is the energy acquired by the particle moving through the field and its gradient. At room temperature the thermal energy $kT \cong 0.026\,\text{eV}$. A voltage drop from an externally applied source across the membrane liquid boundary on the order of $2 \times 10^{-3}\,\text{V}$ would be required in order to make the drift current significant with respect to the total diffusion current under these assumptions. One way in which smaller drift currents and smaller voltages could be significant is if the ions with low velocities perpendicular to the membrane are the most important in binding to the membrane. Slow molecules stay close to the membrane for longer times, and these molecules are most affected by the applied forces [6].

For different boundary conditions the results will be quite different. If, for example, the boundary was nearly perfectly reflective, then the concentration gradient would be nearly 0, and so would the net diffusion current. Additionally, the gradient in the concentration may occur over a larger distance than the gradient of the electric field. At steady state the concentration at the membrane can be expected to increase until the diffusion current and the drift current balance each other so that the net current is equal to the rate at which the molecules are bound to the membrane or pass through it.

There are four forces that may become important when considering the interaction between two particles in a fluid. These are the osmotic diffusion force, the electrostatic force, the van der Waals force, and the hydration force [9]. These forces may all become important in considering the interaction between particles or bilipid membranes in an aqueous fluid. Electrostatic or coulomb forces between particles of like charge are repulsive. Because the charged particles attract free ions of the opposite sign—which produces a double layer—they are effectively shielded or are screened by the charged ions of the opposite sign when immersed in a conducting fluid. This force decays exponentially or

$$\vec{F}_c = \vec{F}_0 \exp - \frac{r}{\lambda_d} \tag{5.34}$$

where λ_d is known as the Debye screening length [11]

$$\lambda_d = \left[\frac{2q^2 n}{\varepsilon kT}\right]^{1/2} \tag{5.35}$$

where n is the density of the ion species doing the shielding, q is the charge and ε is the dielectric constant of the solution, k is Boltzmann's constant, and T is the absolute temperature. For physiological saline solution of approximately 0.14 M, the Debye length is approximately 0.83 nm [12]. Thus, the electrostatic forces are important only at very short ranges.

For like particles, the forces are repulsive at short distances (0.1 to 0.2 nm) and attractive at longer ranges. These forces may be thought of as being generated by transient electromagnetic fields because of fluctuations that occur as a result of thermal agitation or natural uncertainties in the position and momentum of the electrons and atomic nuclei.

If one thinks of the local transient fluctuations in terms of the underlying contributions from oscillations at all possible frequencies, it can be shown that the strength of the contributions due to the local fluctuations at a given frequency is proportional to the absorption of light at that frequency by the material. For an individual atom these forces fall off very rapidly as $1/r^7$ [7]. However, when they are integrated over the surface of a membrane, which is thick compared to an atomic layer, they are correlated over many atoms, as the wavelengths are large compared to an atomic diameter.

A calculation of these fields has been performed starting with quantum field theory [13]. The size of the forces and the rate at which they decay depend on the distance between the membranes and the difference of the bulk polarizability of the membrane and the aqueous gap in a complex way. All frequencies of the charge fluctuations contribute to the attraction, and each gives rise to a different relationship between energy and the distance of separation. For many simple cases and for a classical explanation of these forces and potential distributions, see Ref. [14].

One case of interest is for two membranes with a distance d_w across the aqueous gap between them. The thickness of the membranes is assumed to be large compared to the spacing. The force between these two membranes is approximately given by

$$\vec{F}_w = \frac{H}{6d_w^3} \tag{5.36}$$

where H is the Hamaker coefficient [9]. In a typical situation, the distances over which the van der Waals force is estimated to be important extend out to separations of 10 to 20 nm, which is substantially longer than a Debye length or the rate of falloff for the electrostatic or coulomb forces. The hydration forces are repulsive forces that rise extremely rapidly as the membrane bilayers approach a separation distance of approximately an atomic spacing. Experimentally, these forces can be expressed in the form [9]

$$\vec{F}_H = \vec{F}_{H_0} \exp -d_w/\Lambda \tag{5.37}$$

where Λ is a scaling constant. In the case of egg phosphomonoesterase bilayers, $\vec{F}_{H_0} \approx 7 \times 10^{-13}$ N/m^2 and $\Lambda = 0.256$ nm. This force may be important up to about 2 nm and is assumed to come about as a consequence of the work required to remove water from the hydrophilic surface of the membrane.

Long-range attractive forces have been observed between hydrophobic surfaces [15]. These forces are proportional to the contact area and may be the orders of magnitude larger than the van der Waals forces. They may also have decay lengths up to 25 nm. The magnitude and range of these forces depends on the temperature and the length of the surfactant's chain, and they appear only when the chains are in a fixed ordered state. These forces appear to be generated when the fields emanating from one surface induce a larger polarization in the other surface layer than in the intervening medium. Some relatively complex expressions for these attractive forces have been worked out [14].

These forces are important in self-organizing processes such as protein folding, ligand binding to hydrophobic receptor sites, and transformation of membrane structures. All these forces act over relatively short ranges in typical biological fluids. The ion densities are so large that charge neutrality is maintained everywhere except very close to charged surfaces.

The effect of an electric field, or an electric field gradient in a fluid, is to superimpose a small drift velocity on a relatively large random thermal velocity. For example, if

we apply an electric field of 10^3 V/m to a Na^+ ion, we would expect a drift velocity of about 5×10^{-5} m/sec as compared to a thermal velocity of about 4×10^2 m/sec. For a protein, we would expect a drift velocity approximately one tenth of the speed of the Na^+ ion, although at higher fields. This means that if we are to transport proteins or other small charged particles over appreciable distances of a few millimeters, we can expect it to take minutes or longer. In the case of bacteria, we have measured drift velocities of 10^{-6} m/sec at 100 Hz in fields of about 10^4 V/m and gradients of 5×10^6 V/m^2 or about 0.2% of the velocity of the Na ions in the same field [5,16].

This drift velocity may also change chemical reaction rates if the rate is limited by the availability of one of the charged components. Consider the case of a chemical reaction that takes place in a homogenous fluid if the chemical reaction has the form

$$(A) + (B) \underset{k_2}{\overset{k_1}{\leftrightarrows}} (C) \tag{5.38}$$

where (A) and (B) are the concentrations of the two input chemical reactants and k_1 is the reaction rate for A + B to C and k_2 is the rate for the back reaction of C to A and B. If we simplify the system and let k_2 be small, then the initial reaction rate may take the form [17,18]

$$k_1 = k(A)^n(B)^m \tag{5.39}$$

where n and m refer to the order of the reaction. In order to find the values of n and m, one can make the concentration of one of the reactants small so that it takes the form

$$k_1 = k(A_0)^n(B)^m \tag{5.40}$$

where we have made the concentration (A_0) large enough so that it is approximately constant, and the changes in the reaction rate can be measured by varying (B). The value of k is given by

$$k = zpe^{-\Psi/RT} \tag{5.41}$$

where z is the collision frequency and p is the steric factor, which is <1 and reflects the fact that not all collisions occur with the right orientation of the molecules to react. ψ is the activation energy, R is the gas constant, and T is the absolute temperature. For many cases the collision frequency is proportional to the current density, and thus there are terms that are proportional to both the drift and the diffusion currents. For example, consider the case of an enzyme reaction on a charged substrate such as a biological membrane. The total current density for a given ion in the fluid incident on the membrane is given by Equation 5.10.

If the chemical reaction rate is limited by the number of ions arriving at the membrane surface with enough energy to overcome the barrier required to initiate the reaction, then a DC drift current may either add to or subtract from the diffusion current. If the field direction is such that it prevents the ion from reaching the surface, then the chemical reaction is blocked. If the direction is reversed, the rate can grow exponentially. These changes in chemical reaction rates with the direction of the electric field are likely to be responsible for changes in the growth and reabsorption of neuritis [19]. They are also likely to be involved in the mobility of cells such as leukocytes and fibroblasts [20,21].

An AC drift current will add to the diffusion current. For the AC fields, the drift current can be thought of as increasing the volume covered by a particle executing a random walk as a result of Brownian motion. Thus, in an asymmetrical environment an electric field oscillating in the x direction may increase the number of particles that will strike the $y-z$ plane in a fixed period of time and can increase the chemical reaction rate for a catalytic reaction at the $y-z$ plane. Seto and Hsieh show that AC fields as low as 5 V/m can increase enzyme reaction rates by a factor of 5 [22]. For a 60 Hz field, the peak-to-peak displacement for Ca^{2+} resulting from this field is estimated to be about 1.6 nm or about twice the thickness of the Debye layer. AC magnetic fields have also been shown to change the growth rate of corn roots at fields levels of 5×10^{-3} T. It is likely that these fields are inducing significant currents [23].

An additional mechanism by which AC or DC electric or magnetic fields can effect chemical reactions is by shifting the energy level and the distribution of particles in them. DC electric fields can shift the energy level by an amount that is given by the change in the dipole moment, $\Delta\vec{M}$, and in the polarizability, $\Delta\alpha$, associated with the transition. A DC field can either stretch or compress a dipole depending on its orientation with respect to the field, thus increasing or decreasing the energy levels for atoms or molecules with different orientations. It also can modify its rate of rotation, speeding it up when the dipole is pointed in the direction of the field and slowing it down when it is pointed away from the field [24]. In a vacuum the modifications of the rotational states have been worked out from the quantum mechanics for relatively simple molecules and can lead to a relatively complex set of allowed energy states that are a function of the applied field [23]. In a solid or a membrane the energy levels between the states corresponding to the different orientations shift, by different amounts, for each state as a function of the applied field. This is known as the Stark effect [25]. The frequency corresponding to this energy shift with a fixed orientation is given by

$$h\Delta f = -\Delta\vec{M} \cdot \vec{E} - \frac{1}{2}\vec{E} \cdot \Delta\alpha \cdot \vec{E} \tag{5.42}$$

where Δf is the frequency splitting between levels, $\Delta\vec{M}$ is the change in the dipole moment, $\Delta\alpha$ is the change in polarizability, and h is Plank's constant. These terms give the linear and quadratic Stark effects for a transition in a uniaxially oriented system. These energy levels will be inhomogenously broadened by the random orientation of the dipoles with respect to the applied field and by the thermal energy. Since the quantum of energy, hf, at microwave and lower frequencies is very much smaller than a quantum of thermal energy, low-lying energy levels are approximately equally populated. However, higher-energy states may be preferentially excited by chemical reactions or optical photons so that different excited states may contain different populations. These states may be further defined by the magnetic field and separated by a Zeeman splitting. Thus, radio- and low-frequency fields corresponding to energy separation between these states may excite transitions between levels that are separated by the Stark splitting and change the population distribution in these excited states. The transition rate between an excited molecule and its final product depends on the overlap between the energy levels of the two states. Thus, the application of an electric field can shift the energy levels so as to either increase or decrease this overlap and the transition rate. This has been discussed at length in Ref. [23] for the case of Zeeman splitting of the energy levels by a DC magnetic field and free radicals [26]. See also Chapter 6 in this volume by S. Engstrom.

5.4 Biological Amplification

Biological systems are not in a state of thermal equilibrium. In a typical cell, energy is supplied by hydrolysis of an ATP molecule, which leads to the pumping of three sodium ions out of a cell and two potassium ions into the cell. The net result is creation of potential difference between the inside and outside of a cell in the range of 50 to 100 mV so that the interior of the cell is at a negative potential with respect to the external environment [27]. This potential difference can be used to amplify a variety of external signals just as a typical electronic amplifier can use a small AC signal to convert DC energy into a larger AC signal. For example, the input from many dentric junctions can be summed in a pyramidal cell to trigger an action potential that is larger than any of the input signals [28]. The input from a single synaptic junction might change the cell resting potential by 0.5 to 1 mV, and 10 to 20 inputs might be required to fire an action potential of 50 to 100 mV [27]. Additionally, subthreshold inputs can lead to the release of neural transmitters that, in turn, can release from 2 to 10,000 Ca^{2+} ions from internal stores. These neural transmitters may remain bound to the postsynaptic membrane for up to 4 sec and reduce the threshold for the firing of successive pulses [29]. Feedback from the postsynaptic membrane to the presynaptic membrane can further reduce the firing potential for the synaptic junction.

Another mechanism of amplification that may be of interest is the extraction of energy from a high-frequency signal. If a low-frequency electric field is added to a higher-frequency field and is incident on a nonlinear reactance, then the low-frequency signal may be amplified parametrically. This mechanism for amplification is valuable in the optical region for the generation of tunable signal sources and for low-noise microwave amplifiers [1,30]. In a biological system the low-frequency signal might be generated by an ongoing process such as the heart and amplified by mixing with an external signal from a power line field.

An additional mechanism for amplifications is stochastic resonance. Stochastic resonance differs from the foregoing mechanisms of amplification in that the energy is extracted from the noise. Consider, for example, a small, externally applied sinusoidal electric field incident on an ion in a potential well. If the energy acquired from the external signal is not large enough to exceed the potential barrier, the ion stays trapped in the potential well. However, if noise is added to the system, then when the sum of the applied electric field and the noise are large enough to provide enough energy to exceed the height of the potential barrier, the ion may escape the potential well. This happens most frequently at the peaks of the applied electric field so that the signal is amplified at the applied frequency. Gains on the order of 20 to 30 dB and increases in the signal-to-noise ratio of 18 dB have been observed for stochastic resonance amplifiers [31]. For an extensive review of this subject and some application neuronal systems, see Gammaitoni [32]. For a bistable system, such as a pacemaker cell that is driven by both noise and a periodic signal, it has been shown that the signal-to-noise ratio can be enhanced by the addition of noise to a weak periodic signal and that power can be extracted from the noise. A strong periodic signal can be generated at signal-to-noise ratios <1 [31,33]. This phenomenon occurs when two energy states are separated by a barrier, and the probability of a transition increases exponentially with increasing noise power. For periodic signals that are insufficient to cause a transition over the barrier but periodically increase the energy of the particle, the transition rate at the signal frequency first increases with increased noise power up to some maximum. When the noise power is increased above this level, the output signal becomes more random (see also Chapter 9 in this volume by Weaver and Bier).

5.5 Effects of Electric Fields on Cell Membranes

Electric fields play a very important role in the normal biological functioning of membranes. Membranes are complex structures containing lipids, voltage-activated ion channels, and proteins. It would be surprising if externally applied fields did not affect the membrane behavior. First, an electric field exerts a mechanical force on a membrane by means of the force exerted on charges in the Debye layer on either side of it and on charged proteins that may protrude from the lipid bilayer. Note that although as a first approximation the membrane is often modeled as a smooth planar or spherical surface, it is highly inhomogenous, and the charges are sparsely disturbed. Thus, the field on a protein may be widely different from the average field. See Figure 5.1a. and b for a partial indication of a membrane and cell complexity. The effects from fields in the plane of the membrane, where large molecules such as proteins are free to move as in a viscous fluid, are significantly different from the effects of fields in the transverse direction, where the membrane components are bound in a layer typically 5 to 15 nm thick.

The field distribution incident on a particular part of a cell membrane is a function of its geometry, frequency, and the cells around it. As can be seen from the models in Figure 5.1d, a wide variety of environments may exist. The currents that flow through and along the membranes are dependent on the geometry and frequency. A variety of equivalent circuits have been used to model both the impedance of the membrane and the extracellular fluids. The simplest of these are a resistor and capacitor in parallel. At very low-frequencies a collection of cells can be modeled with resistors as indicated in Figure 5.1c.

The interiors of cells are normally negatively biased in relation to the surrounding fluid by 50 to 150 mV, which leads to average transverse electric fields up to tens of millions of volts per meter [34]. The effective membrane resistance (R_m) per unit area takes on values of 0.14 to 15 Ω/m^2 in the transverse direction. This corresponds to resistivities in the range of $\rho_m = 10^7$ to 10^9 Ω m. The relative dielectric constant for the membrane is typically in the range of 2 to 4. Both the surrounding fluid and the interior of a cell have resistivities ρ_f of about 2 Ω m and a relative dielectric constant of 50 to 80. This means that the cell membrane tends to shield the interior of a cell very effectively from externally applied fields at frequencies below a few kilohertz and becomes almost a short circuit in the multimegahertz region of the spectrum. In most cells the interior of the cell contains complex structures that are functions of time as the cell grows and divides. See Figure 5.1b.

Consider the case of an oversimplified hypothetical rectangular cell as shown in Figure 5.1c. At low-frequencies, an external field $\vec{E}$ causes a current density $\vec{J}_f = \vec{E}/\rho_f$ to flow in the external medium, where ρ_f is the resistivity of the fluid. The corresponding voltage drop is $V = \vec{E}L = \vec{J}_f\rho_f L$, which we can consider to be applied to the cell. This voltage is distributed across the cell length as

$$V = [\rho_m 2t + \rho_f(L - 2t)]|J_m| \tag{5.43}$$

where $\vec{J}_m$ is the current density through the cell and ρ_m is the resistivity of the membranes. Typical cell membrane thicknesses are 6 to 10 nm, and typical dimensions are 10 to 150 μm. Setting $L = 100$ μm and

$$\rho_m 2t = 10\,\Omega m^2 \tag{5.44}$$

$$V = (10\,\Omega m^2 + 2 \times 10^{-6}\,\Omega m^2)|J_m| \tag{5.45}$$

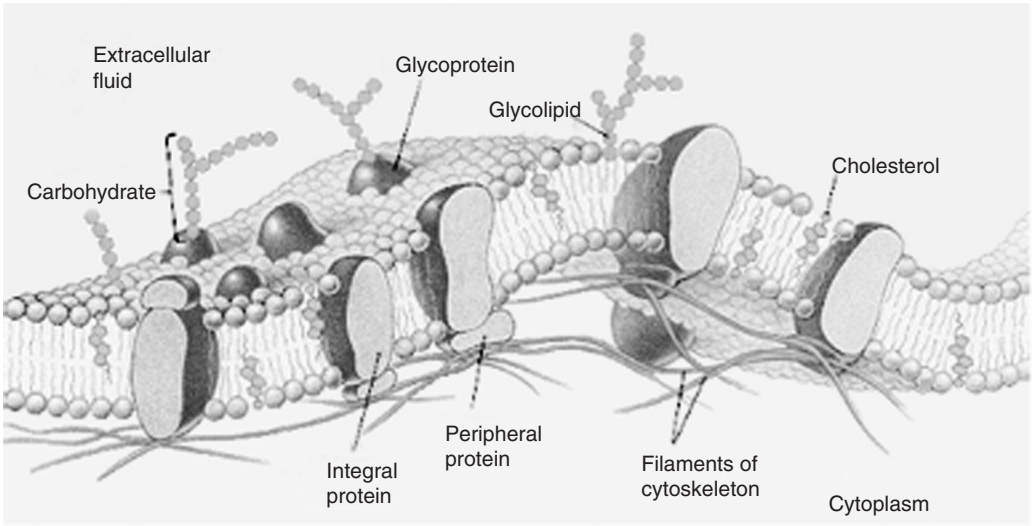

(a)

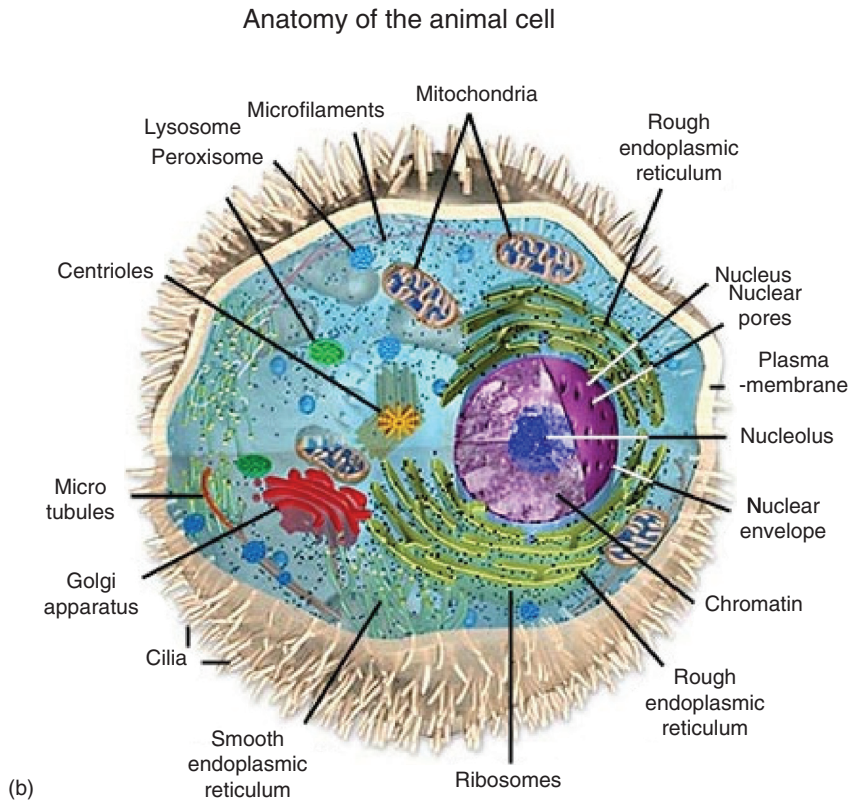

(b)

FIGURE 5.1 (See color insert following page 380.)
(a) Model of a cell membrane. (From Chiras, D., *Human Biology*, © 5th edition, 2006, Jones and Baretlett Publishers, Boston. With permission.) (b) Anatomy of the animal cell. (From *Molecular Expression*, http://microscopy.fsu.edu, accessed Sep. 30, 2005; drawing © M.W. Davidson and Florida State University. With permission.)
(*continued*)

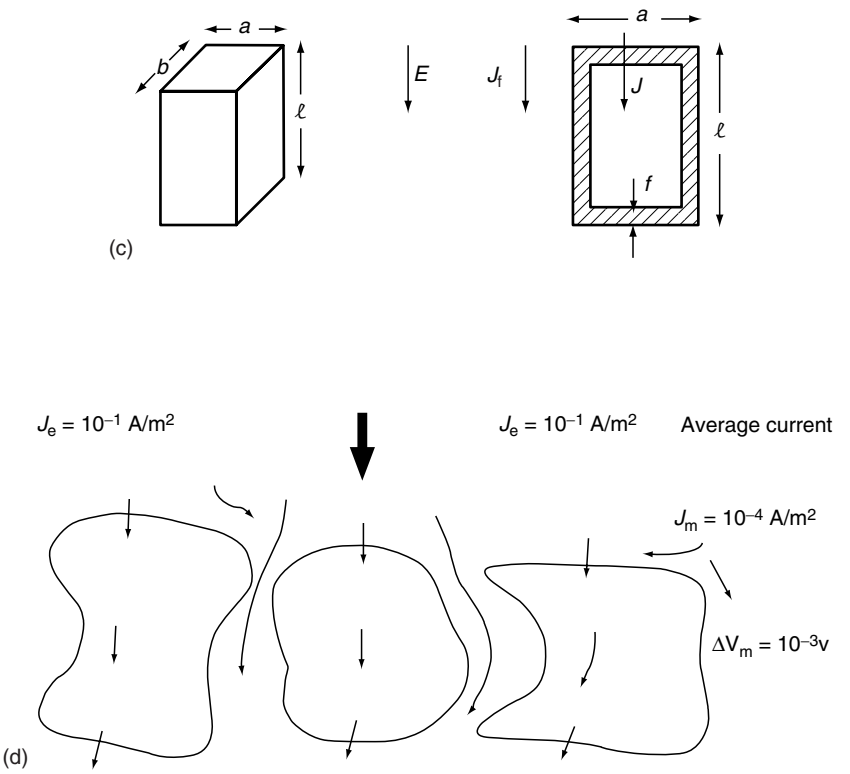

FIGURE 5.1 (continued) (See color insert following page 380.)
(c) Current distribution in a hypothetical rectangular cell. (d) Partition of 60-Hz currents through and around cells for an average current density $J = 10^2$ A/m^2. J_c is the current density between cells, and J_m is the current density through the membrane. (From Wachtel, H., private communication. With permission.)

This shows that essentially all of the transverse voltage drop occurs across the membrane at low-frequencies and the interior of the cell is almost completely shielded from external fields. A more complete theory for long cells that accounts for the internal resistance of the cell is given by Cooper et al. [35]. See also Chapter 11 by Pila [114]. Note that muscles, nerves, and a number of other cells may be much longer than 100 μm and may have dimensions in centimeters. Additionally, blood vessels form long, low-resistance paths that may concentrate currents due to externally applied fields. The anisotropic characteristics of cells are reflected in an anisotropy of the dielectric and conductive properties of tissue, which may give variations of as much as 10 to 1 in conductivity, depending on the direction of measurement relative to cell orientation [36]. A number of fish, including sharks, have been shown to use very long cells and to sum signals in both series and parallel to increase the voltage drop across a sensitive membrane in order to sense fields as low as 10^{-6} V/m [37–39]. The long cell may be thought of as an antenna that concentrates the field across a very thin, voltage-sensitive detector membrane. This membrane appears to have a built-in amplifier that allows detection of signals that are only a little above the natural electrical noise.

Membranes are not just simple linear resistors, but they usually are nonlinear and, in the case of nerve cells, are time varying as well. For a passive membrane in which the membrane potential is primarily determined by the concentration gradient of a single ion such as K^+, the Nernst equation predicts a diode-rectifying characteristic of the form [31]

$$I = I_0\left[\exp\left(\frac{V_m}{\eta V_T}\right) - 1\right] \tag{5.46}$$

where V_T is given by

$$V_T = \frac{kT}{q} = 0.026\,\text{V} \tag{5.47}$$

at $T = 300\,\text{K}$. q is the charge on the electron, V_m is the voltage across the membrane, I_o is the current for ideal back-biased current in amperes, and η is a dimensionless constant. Thus, for currents flowing through a membrane in one direction, the current is nearly constant, whereas for flow in the other direction the currect increases exponentially with voltage. In addition to passive currents, cells also use the energy from metabolic processes for the active transport of ions against the fields established by the concentration gradients. These processes are usually modeled as current sources and described as pumps [31]. A thermodynamic approach to pumping shows that ions can be pumped if they form a compound with a material that can flow through the membrane and that is created on one side of the membrane and destroyed on the other [40]. A large variety of models have been generated to characterize the effects of externally applied fields on the transport of ions through membranes [41–43]. However, the details of the pumping process are not well understood. In addition to ion transport, electrical fields can change the binding of ions or molecules to the membrane surface.

In the case of pacemaker cells, there are also feedback processes that lead to an oscillating membrane potential and a membrane resistance that is a function of time. The current flow for these cells is described empirically by the Hodgkin–Huxley equation [31]. An alternate approach that treats the nerve pulse like a plasma instability has been proposed by Triffet and Green and Vaccaro and Green [44,45]. Na^+ and K^+ currents are the dominant carriers for the propagation of nerve impulses along a cell. It is generally believed that the Na^+ and K^+ currents that flow through the membrane in opposite directions are carried through separate channels. Ca^{2+} ion currents are involved in the activation of at least a portion of the K^+ currents and are voltage gated. By activating the K^+ currents, the Ca^{2+} ions shorten the length of time the cell is depolarized and thus speed up the firing cycle [46]. A statistical approach to the formation of protein channels in the membrane by Baumann and Easton predicts many of the observed characteristics [47–49].

During the firing of a nerve cell, the Na^+ current pulse precedes the K^+ current pulse, which returns the cell to its resting potential [31]. The overall concentration balances are maintained by active ion pumps. Cl^- Mg^{2+}, and possibly OH^- and H^+ ions may also be involved in the current flow across a cell membrane.

The firing of a nerve cell typically involves voltage spikes of $10^{-1}\,\text{V}$ and peak current densities of $1.5\,\text{A/m}^2$. Changes in the firing rate can be induced by the injection of charge through a microelectrode of $<10^{-9}\,\text{A}$ for a few milliseconds. However, in cases where electrodes are used to stimulate muscles or to control epilepsy, the current is injected through a series of cell membrane fluid boundaries at a distance from the controlling nerve fiber. Thus, typical injected currents to produce behavioral changes in cells are in milliamperes, and current densities are $10\,\text{A/m}^2$ or higher.

For fields parallel to the plane of the membrane, it is possible to obtain electrophoresis or a rearrangement of charged particles. This has been shown by Poo in a striking fashion in cultured embryonic *Xenopus* myotomal muscle cells [50,51]. Receptors on the surface of the cell were labeled with a fluorescent dye and allowed to uniformly distribute themselves. Exposures to electric fields of 10^2 to $10^3\,\text{V/m}$ were sufficient to concentrate the

fluorescent-labeled receptors on the side of the anode in about 10 min. After shutting off the field, diffusion returned the dye to its uniform distribution in about 2 h. This corresponds to an in-plane diffusion constant of about $3 \times 10^{-12}\,m^2/sec$. The force on the receptor molecules or particles in the membrane includes not only $q\vec{E}$ but also any viscous drag that may be generated by the flow of ions of the opposite sign moving along the surface in the opposite direction. The direction of motion for a given charged particle seems to depend on whether it has a larger or smaller zeta (ζ) potential than the potential across the charged double layer at the interface between the cell surface and the fluid (see Equation 5.16).

Additional work has shown that the distribution of acetylcholine (ACh) receptors is changed by external fields [48,49]. These receptors are concentrated on the cathode-facing surface of the cell in fields of $10^3\,V/m$ over a period of 30 min by literally rearranging channels already existing in the cell membrane. The concentration or clustering persists for at least 5 h after the field has been turned off, indicating that the clustering is relatively stable. Single-channel patch measurements show both a higher density of ACh channels in the clusters near the cathode and a longer mean duration of the pulses through the transmembrane channels. The length of the current pulse near the anode does not differ from the controls, indicating that the field itself does not have a direct effect on the channel kinetics. The lateral diffusion coefficient, D, of ACh receptors in the plasma membrane of cultured *Xenopus* embryonic muscle cells is estimated to be $2.6 \times 10^{-6}\,m^2/sec$ at 22°C [48,49]. Lateral concentration gradients in lipid monolayers have been shown to be induced by externally applied electric field gradients. For binary mixtures of dihydrocholesterol and dimyristoylphosphatidylcholine, the application of an electric field gradient at pressures below the critical pressure produces a liquid–liquid phase separation in a monolayer that is otherwise homogenous [52]. This separation occurs at field levels on the order of $10^7\,V/m$ and gradients of 10^9 to $10^{11}\,V/m^2$.

5.6 Nonlinear Effects of AC Fields on Cells

5.6.1 Introduction

The application of an AC electric field to nonlinear systems, which can be described by either a nonlinear resistance or capacitance, leads to at least partial rectification of the input signal and the generation of harmonics. If two or more signal frequencies are applied, it also leads to frequency mixing of the form

$$f_o = \pm mf_1 \pm nf_2 \tag{5.48}$$

where f_o is the output frequency, f_1 and f_2 are input frequencies, and m and n are integers. The rectified component of the AC current can, in turn, lead to ion accumulation at interfaces, which results in changes in ion concentration [53,54]. These changes in ion concentration, in turn, can affect biological function. Another important additional effect is the dependence of the dielectric constant on frequency. This leads to changes in the electric field distributions in tissue with frequency. Thus, both the electrophoretic and the dielectrophoretic forces become both size and frequency dependent. A third—possibly important—additional effect is the excitation of frequency-sensitive biological systems in a resonant manner. By driving systems near their resonant frequency, we may change the effective amplitude of the stimulating signal and change the frequency of the nerve cells firing.

In this section we will review the rectification process at the cell membrane in some detail. Additionally, we will show that cell nonlinearities lead to frequency-dependent effects such as injection phase locking of pacemaker cells. We will also briefly examine some problems associated with the exposure of cells to very low, extremely low-frequency (ELF) fields and the application of large ELF fields to biological systems.

5.6.2 Rectification by Cell Membranes

The rectification of currents flowing across membranes has been studied by many authors, beginning with Katz in 1949. Much of this work is referenced by Hayashi and Fishman in their paper on the inward rectifier K^+ channel kinetics [53].

For many passive cell membranes, an approximate relation for the transmembrane current can be derived from the Nernst equation as given in Equation 5.41 [31]. If we apply an AC signal across the membrane of the form $V_M = V_0 + V_1 \cos \omega t$, the resulting current can be approximated for small values of V_M (i.e., $qV_M < \eta kT$) by a Taylor series yielding

$$I = \frac{I_0}{\eta V_T}\left(V_0 + \frac{V_1^2}{4\eta V_T} + V_1 \cos \omega t + \frac{1}{4\eta V_T} V_0 V_1 \cos \omega t + \frac{V_1^2}{4\eta V_T} \cos 2\omega t + \cdots\right) \tag{5.49}$$

It is to be noted that the second term in the expression is the first approximation to the fraction of the applied AC voltage V_1 that yields a DC current component ΔI,

$$\Delta I = \frac{I_0}{4}\left(\frac{V_1}{\eta V_T}\right)^2 \tag{5.50}$$

or an offset voltage V_{DC} given by

$$V_{DC} \approx \frac{I_0}{4}\left(\frac{V_1}{\eta V_T}\right)^2 R_m \tag{5.51}$$

where R_m is the membrane impedance. This predicted voltage offset for an applied AC current has been measured by Montaigne and Pickard [55]. In their experiments, an AC signal was applied to a large plant cell by a strip line, and the measured voltage shift was obtained through microelectrodes located outside the applied AC fields. For an applied AC field of about 0.2 V, they measured a DC offset of 1 to 2 $\times$ 10^{-4} V. For frequencies above 2.5 kHz, the effects of the membrane capacitance must be taken into account, and the effective driving voltage is reduced to

$$(V_1)_{eff} = [\sqrt{2}\, a\sigma_e\, \vec{E}_{1rms}][(\sigma_e + aG)^2 + (a\omega C)^2]^{-1/2} \tag{5.52}$$

where a is the cell radius, σ_e, is the conductivity of the medium $\vec{E}_{1rms}$, is the electric field strength in the medium surrounding the cell, G is the membrane conductance per unit area, ω is the frequency, and C is the membrane capacitance per unit area [56]. This leads to the usual roll-off in the measured DC offset with increasing frequency. Note that the DC effect gets still smaller at higher frequencies (above 1 MHz) because of transit time limitations for ion flow across the membrane [57].

The relaxation times for a typical K^+ channel in an *Aplysia* membrane has been measured to be from 2 to 8 ms [51]. Rectification has also been demonstrated in thin lipid membranes [58]. In these systems, both the conductivity of the membrane and the ion concentration differences across it can be controlled. The Nernst equation was shown

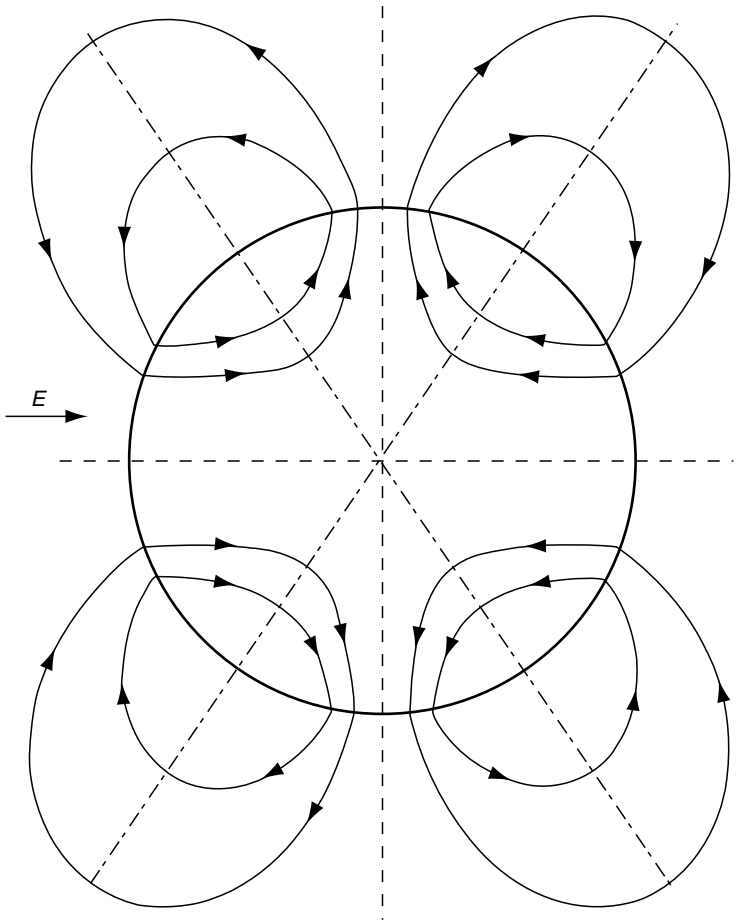

FIGURE 5.2
Induced DC current distribution in a spherical cell. (From Bisceglia and Pinto, I., personal communication, 1984. With permission.)

to apply to the I vs. V curve over a range of voltages from -60 to $+40$ mV. Depending on the ion concentration and membrane doping, the values of η ranged from 1 to 0.25.

A different treatment of the nonlinear response of passive cell membranes to an applied AC field has been carried out by Franceschetti and Pinto and by Casaleggio et al. [59,60]. Both these groups have expanded the Nernst equation in a Volterra series that takes into account memory of the preceding state of the cell. They have also treated the cell in spherical rather than planar geometry. The inclusion of a spherical cell requires that the total current into and out of the cell be equal to zero, and thus loops are formed circulating through the cell membrane (see Figure 5.2). All the theoretical treatments predict a DC component that varies as the square of the input signal V and tends to hyperpolarize the cell or make the interior of the cell more negative.

Cain has considered the effects of an AC field on nonlinearities of the nerve cell by numerical analysis of the Hodgkin–Huxley equation [61].* He applied a voltage

*Bisceglia and Pinto have applied a Volterra series expansion to the Hodgkin–Huxley equations. This approach gives an alternate method to Cain's of computing the current shifts resulting from applied AC signals [62].

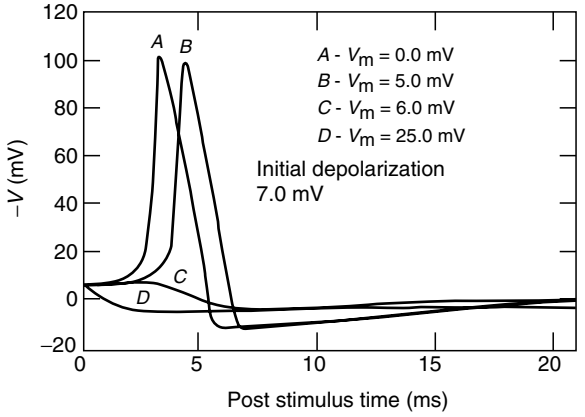

FIGURE 5.3
Computed membrane action potentials in response to an initial membrane depolarization of 7 mV for different values of V_m. Curves are solutions to the Hodgkin–Huxley equations. (From Cain, C.A., *Bioelectromagnetics*, 2, 23, 1981. With permission.)

$$V_m = V_0 + V_1 \cos \omega t[u(t) - u(t - \tau)] \tag{5.53}$$

across the membrane, where $u(t)$ and $u(t - \tau)$ are unit step functions that define an AC pulse of length τ. For the case where the AC frequency is large compared to the reciprocal of the pulse length, if a 7 mV depolarizing pulse is also applied to the membrane, the action potential is obtained as shown in Figure 5.3. Cain has assumed coefficients appropriate to the giant squid axon. Increasing V_1 first delays, and then suppresses, the action potential. If no depolarizing pulse is applied, the predicted changes in g_{Na} and g_K and the deviation V from the resting potential are as shown in Figure 5.4 for a 10 msec AC pulse with $V_1 = 25$ mV. Note that the applied AC frequency is assumed high enough not to be resolved in these figures. From these results, it is clear that AC signals can induce substantial changes in the operating characteristics of nerve cells at moderate to high levels of applied voltage. Although the appropriate coefficients were not measured in order to make a direct comparison between theory and experiments, Wachtel's results on *Aplysia* at frequencies above the lock-in range would appear to support Cain's theoretical predictions [63].

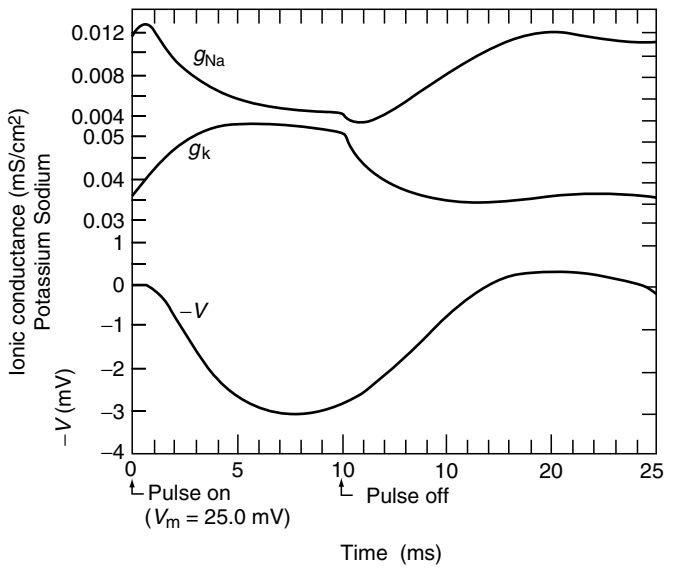

FIGURE 5.4
Response of model axon to a pulsed oscillating component of membrane electric field (10-ms pulse, V_m = 25 mV). The membrane potential and the sodium and potassium conductances are shown. These curves are solutions of the Hodgkin–Huxley equations. (Note: 1 mS/cm^2 = 10 S/m^2.) (From Cain, C.A., *Bioelectromagnetics*, 2, 23, 1981. With permission.)

Wachtel has made a series of measurements that demonstrate the nonlinear characteristics of pacemaker cells from *Aplysia* [61]. First, he measured the current input through a microelectrode that changed the firing rate of the cell. The current threshold for a minimum detectable change was approximately 6×10^{-10} A at frequencies between 0.8 and 1 Hz (see Figure 5.5). The natural firing rate for this cell is about 0.8 Hz, and an increasing current is required to synchronize the cell to the injected signal as the frequency deviates from the natural firing rate. A theory for injection locking of electronic oscillators predicts that the signal required for locking an oscillator to an external signal increases linearly as the difference between the two frequencies $\Delta\omega$ increases [64]. The signal required for lock-in according to this theory is given by

$$I_t \approx |A\Delta\omega|\ I \tag{5.54}$$

where I_t is the injected signal current and I is the peak unperturbed oscillator current. $A = \partial\phi/\partial\omega$ is the rate of change of phase with respect to frequency in the unperturbed oscillator. $\Delta\omega_0$ is equal to the difference between the frequency of the free-running oscillator and the injected signal. This expression is applicable as long as

$$\Delta\omega_0 \leq \frac{2\pi}{\tau} \tag{5.55}$$

where τ is the time constant for adjusting the gain of the circuit. The time constant τ for the *Aplysia* cells varied between 0.1 and 0.5 sec, and this corresponds to a maximum measured lock-in frequency of about 10 Hz. The results in Figure 5.5 show the threshold for one-to-one locking up to about 2 Hz. In the range from 2 to 10 Hz, Wachtel observed a lower threshold for subharmonic locking than one-to-one locking. At frequencies above 80 Hz, he observed a constant shift in the firing rate of the neuron in response to the injected transmembrane AC signal. The natural firing rate would be restored by also injecting a transmembrane DC signal equal in amplitude to about 1% of the peak-to-peak value of the AC current. This DC current was in the depolarizing direction, making the exterior of the cell more negative with respect to the cell cytoplasm to increase the firing rate (i.e., to restore it to its natural value). Apparently, the applied transmembrane AC current was partially rectified so as to hyperpolarize the membrane (making the interior of the cell more negative with respect to the external fluid). The details of how the applied field modifies the ion flow are only partially understood, but one characteristic is an increase in the conductivity for K^+, which increases its flow out of the cell. Wachtel also

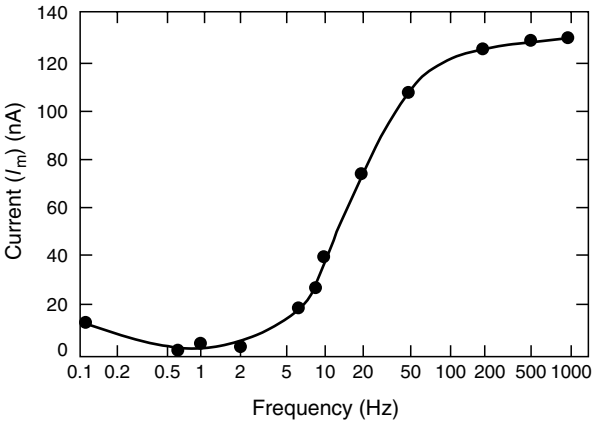

FIGURE 5.5
Intracellular (transmembrane) currents I_m (in nA) needed at different frequencies to produce firing-pattern changes (in a pacemaker neuron). Note that the detectable changes take on different forms at different frequencies. (From Wachtel, H., *Proceedings of the 18th Annual Hansford Life Science Symposium*, Technical Information Center, U.S. Department of Energy, Richland, WA, 132, 1978. With permission.)

injected low-frequency currents into the seawater surrounding the cell preparation through external electrodes [61]. In this case, the minimum current densities flowing in the vicinity of the cell preparation for injection locking were estimated to be about $10^{-2}\,\mathrm{A/m^2}$, and there was about a 30 to 1 variation between the maximum and minimum sensitivities for changes in angle between the applied field and the cells. At frequencies above 100 Hz, a minimum of about $0.35\,\mathrm{A/m^2}$ was necessary to obtain a detectable change in firing rate.

These studies have been extended by Barnes et al., and injection locking at harmonic and subharmonics has been shown to occur. It is suggested that phase locking may provide a mechanism for narrow banding or time averaging so that a weak coherent signal may be distinguished from noise by a cell. In an electronic circuit model we showed we could phase lock an oscillator at signal-to-noise ratios <1 [65]. Extensive modeling of phase locking for a squid axon using two versions of the Hodgkin–Huxley equations has been carried out by Fohlmeister et al. [66]. They show that phase locking can occur for a wide variety of frequencies with AM-modulated signals at injected current densities greater than $0.1\,\mathrm{A/m^2}$ [67]. For natural oscillation frequencies less than the externally applied signal, the system may be treated as a parametric process. For parametric amplification, a phase stability such that

$$\frac{\mathrm{d}\Phi}{\mathrm{d}t} < \Delta\omega - KV_\mathrm{s} \tag{5.56}$$

is required for injection locking of the frequency of oscillation to an external signal, where $\mathrm{d}\Phi/\mathrm{d}t$ is the rate of change of the phase, $\Delta\omega$ is the frequency offset, K is the linear control characteristic in units of $(2\pi\,\mathrm{Hz/V})$ and is closely related to the loop gain, and V_s is the injected signal [68]. Stated in words, this equation requires that the amplified signal, KV_s be large enough to correct for the random frequency fluctuations $\mathrm{d}\Phi/\mathrm{d}t$ generated by the noise for the system to become phase locked to a signal that is displaced by $\Delta\omega$ (see Figure 5.6 for some examples of injection locking of pacemaker cells to an external signal) [65]. An increase in the sensitivity to electromagnetic fields has also been shown in isolated frog hearts for signals that approach the natural resonant frequency or firing rate [69]. In these experiments, the firing rate of the heart was shown to increase as much as 30% when a signal in the vicinity of 10 to 20 V/m was applied through Ringer's solution to the isolated frog hearts at a frequency between 0.5 and 1 Hz. The natural firing rate of these excised hearts started out at approximately 1 Hz and dropped to about 0.5 Hz

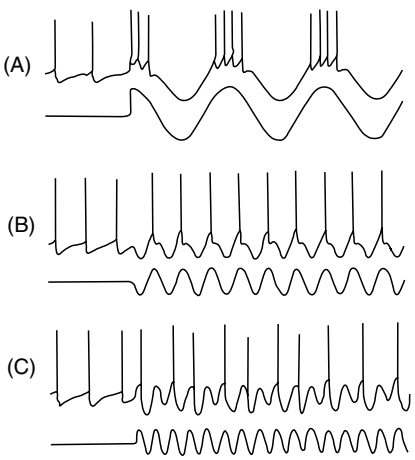

FIGURE 5.6
Examples of several modes of synchrony between an imposed ELF field and neuronal patterns. In each case the ELF current is shown below the transmembrane potential recording. (A) For ELF frequencies well below FR_0, several nerve impulses (spikes) are locked to each ELF half cycle. (B) ELF frequencies slightly above FR_0 are effective in phase locking the rise of neuronal spikes on a one-to-one basis. (C) For ELF frequencies several times greater than FR_0, phase locking can take the form of spikes occurring on alternate cycles (two-for-one synchrony). (From Barnes, F.S., *Bioelectromagn. Suppl.*, 1, 67–85, 1992. With permission.)

over a period of 2 h, where they remained stable for at least 5 h. To get a 30% increase in firing rate at 60 Hz, it was necessary to apply field strengths of 60 to 80 V/m. Thus, we have additional evidence that electric fields with repetition rates near the natural biological signaling frequencies are more likely to induce changes than those of higher frequencies and that signal strengths required for a given shift increase approximately linearly up to some cutoff, as shown in Figure 5.5.

For weak fields, it has been shown that cells can respond differently to signals that are both space and time coherent than they do for signals that look like the background noise. Litovitz et al. have shown that the application of 10 μT magnetic fields at either 55 or 65 Hz doubles the specific activity of ornithine decarboxylase (ODC) in L929 cells if the signals are coherent for periods of 10 sec or longer during the course of a 4 h exposure [70]. The applied signal and the corresponding ODC response as a function of the coherence time are shown in Figure 5.7. The ODC response of the cell can be fitted to an exponential curve of the form

$$(\text{ODC}) = 1 + 1.26\left[1 - \exp\left(\frac{\tau_{\text{coh}}}{\tau_{\text{cell}}}\right)\right] \tag{5.57}$$

where τ_{coh} is the length of the time between shifts in frequency and the introduction of a random phase shift and τ_{cell} is the effective time constant of the cell [70]. τ_{cell} has a value of about 8 sec for these cells. If a spatially coherent noise signal with a power spectral density ranging from 30 to 90 Hz is superimposed on the coherent signal, the increased ODC response decreases with a decreasing signal-to-noise ratio and is less than 10% at a signal-to-noise ratio of 1 [71]. This work has been extended to show that temporally incoherent magnetic fields inhibit 60 Hz-induced changes in the ODC activity of developing chick embryos [72].

For the exposure geometry used in these experiments, the magnetic field induced a corresponding electric field of 4 μV/m. This signal is well below the calculated thermal noise field of 0.02 V/m for a 20 μm cell diameter. The combined results of the experiments cited above indicate that both space and time coherence may be used by cells to separate useful signals from larger natural background noise signals. For example, to get a significant biological response, some threshold number of channels or receptor molecules may need to be activated within a given period of time; this, in turn, requires nearly

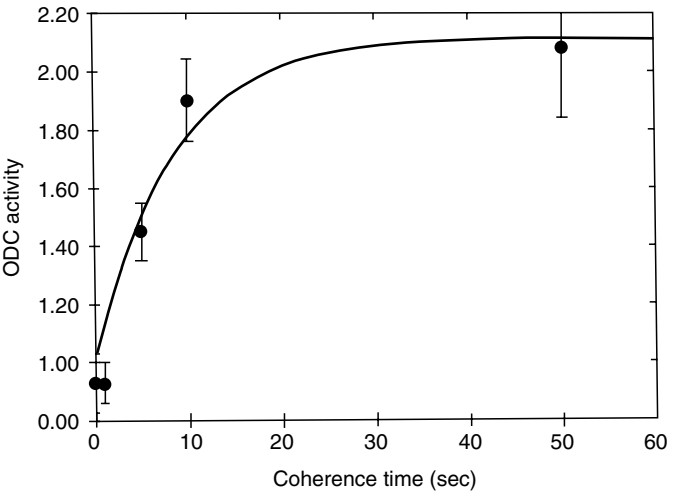

FIGURE 5.7
Plot of the enhancement of ODC activity (exposed/control) as a function of the coherence time, τ_{coh}, of the applied field. The solid line is the best fit to the mathematical function given by Equation 5.44, where τ_{cell} is found to be 8.2 sec. The experimental points shown represent a minimum of six different exposures. (© Academic Press; From Litovitz, T.A., Krause, D., and Mullins, J.M., *Biochem. Biophys. Res. Commun.*, 178, 3, 862, 1991. With permission.)

simultaneous activation over a significant fraction of the cell surface. Similar results have been obtained for developing chick embryos, where weak coherent signals lead to an increased incidence of abnormalities [73]. In this work, Litovitz and his colleagues show an increase in the incidence of abnormalities of approximately a factor of 3 for White Leghorn chicken embryos incubated in periodic magnetic fields with peak field strength of 1 μT (100 Hz repetition rate, 500 μs pulse duration, 2 μs rise, and decay times) when compared with the controls. This increased rate of the incidence of abnormalities was nearly eliminated with the addition of band-filtered noise with a spectrum running from 30 to 100 Hz and a root mean square value of 1 μT. Thus, Litovitz makes a strong case for a requirement of both space and time coherence for biological systems to detect signals below the natural noise environment.

A number of experiments indicate that at least two mechanisms are involved in the effects of low-level time-varying magnetic fields on membrane transport. The first of these is through Faraday's law or the induced electric field, which, in turn, induces electric currents. In these experiments, one would expect to get the same effects by introducing electric fields with electrodes at levels that induce the same current densities. The second group of experiments indicates that the background DC magnetic field is also important and that the combined effects of AC and DC magnetic fields are observed.

The initial experiments by Walleczek and Liburdy showed an enhanced uptake of Ca^{2+} in Con. A-activated rat thymocytes with exposures of 1 h to 60 Hz magnetic fields of 22 mT and induced current densities of 0.16 A/m^2 [74]. In this paper the exposure system consisted of concentric rings on cell culture plates, which, in turn, were placed in a water-cooled solenoid that produced a uniform magnetic field. This was followed by a group of experiments by Liburdy on Ca^{2+} transport across mitogen-activated lymphocyte membranes [75]. In these experiments, both the DC and the AC magnetic fields were controlled so that the DC geomagnetic field and the ambient 60 Hz fields were perpendicular to the exposed and control plates. The results show an increase in the Ca^{2+} influx during the plateau phase of the calcium signaling for Con. A-activated lymphocytes, which was a function of the induced electric field and which could be reproduced by applying the electric fields across the cells with a salt bridge at levels between 0.1 and 0.17 V/m. This corresponds to induced current levels of 0.168 to 0.28 A/m^2 in the fluid surrounding the cells, which had a conductivity, $\sigma = 1.68$ S/m, that is approximately a hundred times larger than the current densities observed around growing cells. Thus, the approximately 20% to 25% increase in the initial Ca^{2+} uptake is the result of a relatively large external current. In other experiments it was also shown that the response is dependent on the age of the animals from which cells are taken [76].

Most other reported experiments have not been done in a way to sort out the differences between possible direct effects of the magnetic fields and the induced electric fields. Yost and Liburdy [77] have also conducted experiments in the same system that show a direct dependence of the calcium uptake on the DC magnetic field.

The experiments by McLeod et al. [78] show both a frequency dependence and a dependence on the electric field strength across the cell membrane. They exposed neonatal bovine fibroblast cells to electric fields in culture through a media bridge. The fibroblasts populated a collagen matrix that enabled the cells to be grown with a dominant orientation and exposed to a well-defined current. An estimate of newly synthesized protein was made by measuring the incorporation of (^{3}H) proline into macromolecules after a 12 h exposure to current densities ranging from 10^{-3} to 10 A/m^2 and frequencies from 0.1 Hz to 1 kHz. The results in Figure 5.8 show an approximately 30% reduction in the ^{3}H counts with current densities as low as 10^{-2} A/m^2. This reduction is interpreted as a reduction in the incorporation of newly synthesized protein into the extracellular matrix rather than as a change in the cell number. The frequency specificity for this threshold is

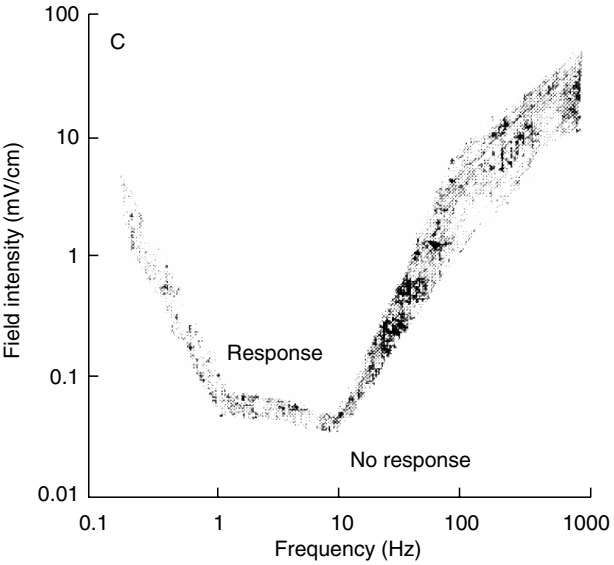

FIGURE 5.8
Minimum field intensity for a detectable response. Summary of results for all tested frequencies and current densities. Current densities were converted to peak field intensities by using the measured media resistivity of 65 Ω cm. The lower boundary of the gray region represents the highest field intensity at which no significant change in extracellular protein accumulation was detected; the upper boundary represents the lowest intensity evoking a statistically significant change ($n = 6$). (From McLeod, K.J., Lee, R.C., and Ehrlich, H.P., *Science*, 136, 1465–1469, 1987.)

shown in Figure 5.8; the peak sensitivity was recorded at $5 \times 10^{-3}\,A/m^2$ and 10 Hz. The corresponding peak electric field intensity was 4.5 mV/m. The fractional change in the (^{3}H) proline was nearly independent of the current density for increases in current density up to two orders of magnitude above $10^{-2}\,A/m^2$. The cell membranes have a resistance many times higher than the resistance of the matrix as a whole. The cells are also asymmetric, with a ratio of major to minor axes of about 7 to 10. Thus, the current through the cell membranes would be expected to be at a maximum when the long axes of the cells are parallel to the applied field. For randomly oriented cells, current densities of $3\,mA/m^2$ produced no significant effect on the rate of proline incorporation. However, when the cells were oriented parallel to the electric field that was estimated at 2 mV/m and 10 Hz, a little more than a 30% reduction was observed. The estimated transmembrane potential was 0.5 μV. With the cell oriented perpendicular to the field, no significant change in proline incorporation was measured at $5\,mA/m^2$.

In addition to the nonlinear conductances associated with Na^+ and K^+ currents, membranes also exhibit nonlinear (i.e., potential dependent) and frequency-dependent capacitances and inductances. It is sometimes useful to think of these effects in terms of a phasor diagram as shown in Figure 5.9, where the electric field vector $\vec{E}$ is rotating at a velocity ω, and ϕ is the phase angle between $\vec{E}$ and the current density $\vec{J}$. If there is, for example, a fixed time delay between the field activation of a current gate and the current flow, then, depending on the frequency, $\vec{J}$ may be in any of the four quadrants and appear capacitive or inductive or even present a negative resistance to an external driving source.

Nonlinear inductive effects seem to be associated with the time delay for the onset of the K^+ currents under excitation in a typical excitable membrane, and they have been studied in the giant squid axon [79]. The nonlinear capacitive effects are difficult to measure at frequencies below a few kilohertz. Extra care needs to be exercised to minimize the series resistance and the end effects of the wire being used to measure the capacitance or inductance. Additionally, corrections must be made in the calculations of the membrane capacitance to take into account the appropriate variations in the frequency response that these terms introduce. However, when this is done, it can be shown that the membrane capacitance has both frequency- and voltage-dependent terms. The capacitance of giant squid axons is shown in Figure 5.10 and Figure 5.11 as a function of frequency and membrane voltage.

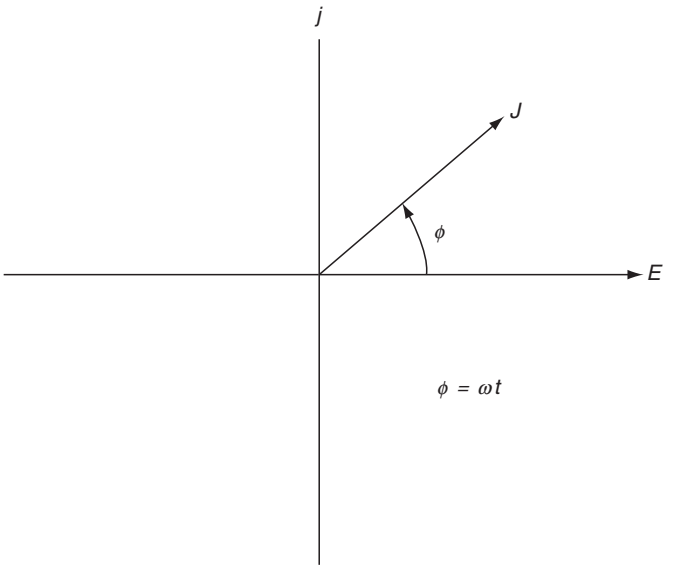

FIGURE 5.9
Steady-state vector characterization of electric fields $\vec{E}$ vs. current density $\vec{J}$ in polar form. ϕ is the phase angle between the sinusoidal electric field $\vec{E}$ and the resulting current density $\vec{J}$.

Variation of the capacitance of these membranes with frequency and amplitude differs from that of a simple bilipid membrane that has nearly constant capacitance. The variation appears to be associated with changes in the conformation of the proteins associated with the Na^+ conductance channels. Nonlinearity in conductance and capacitance can be induced into a bilipid membrane by the addition of Alamethicin. The nonlinear inductance or capacitance may also generate both sum and difference frequencies if two signals are applied. For the case of the single signal, a DC term is added to the current density that is proportional to membrane potential and the square of the applied AC signal [80]. The effects due to nonlinear membrane capacitance thus far observed are small. They

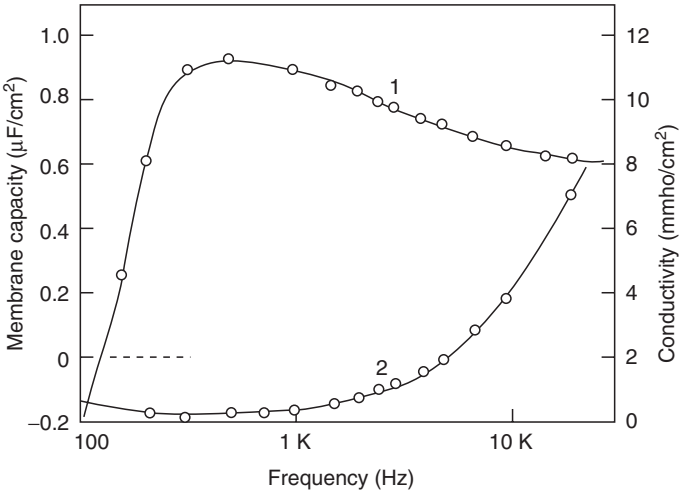

FIGURE 5.10
Membrane capacitance (Curve 1) and conductivity (Curve 2) of squid giant axon at various frequencies. Note the anomalous behavior at low-frequencies. (Note: 1 μF/cm^2.) (From Takashima, S., in *Biological Effects of Nonionizing Radiation*, ACS Symposium Series, No. 157, Illinger, K.H., Ed., 133–145, 1981.)

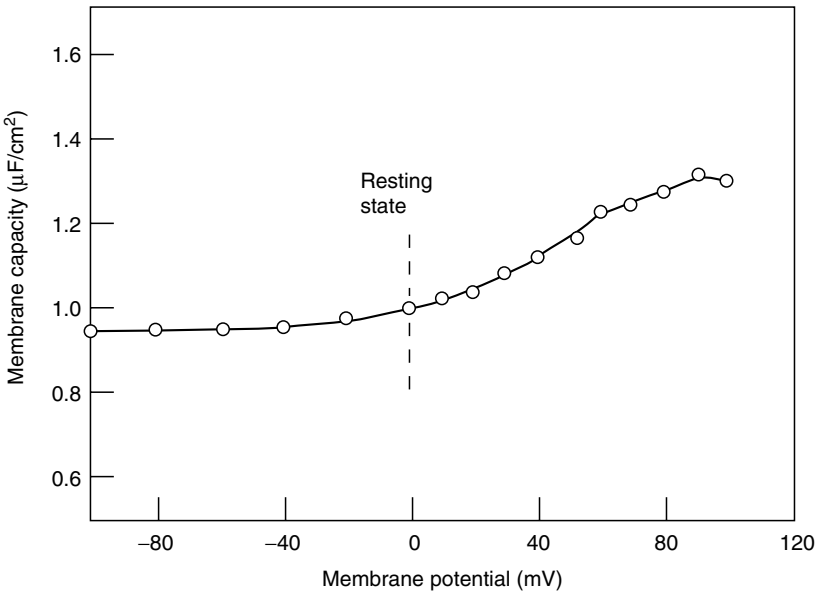

FIGURE 5.11
Membrane capacitance of squid giant axon at various membrane potentials. Membrane potential was shifted by injecting currents. The abscissa shows the actual potential across the membrane in millivolts. (From Takashima, S., in *Biological Effects of Nonionizing Radiation*, ACS Symposium Series, No. 157, Illinger, K.H., Ed., 133–145, 1981.)

appear likely to be more important in providing an understanding of the possible gating mechanism in membranes than as a mechanism for introducing rectification.

Another form of nonlinearity in the electrical response of cells comes about in what is often described as adaptive processes. For example, we found that repetitive exposures of pacemaker cells (taken from the ganglion of an *Aplysia)* to microwave pulses resulted in a decreasing reduction in the firing rate by successive pulses. This kind of change has also been shown to occur in neurons that have been conditioned with repetitive stimulation. Studies of conditioning have shown decreases in potassium ion conductance through membranes, thus raising the internal potential and enhancing the excitability [81,82]. The decrease in resistance between adjacent cells can occur in two ways. First, the resistance of gap junctions may be reduced by repetitive electrical stimulation, which increases the electrical coupling between the cells by up to 62%. Second, repetitive electrical stimulation can modify the chemical excitatory postsynaptic potential by amounts ranging from 31% to 140% [83]. This change is associated with the movement of protein kinase C from the interior of the cell into the membrane. An accompanying change in Ca^{2+} concentrations and the movement of a second messenger, diacylglycerol, into the membrane reduce the potassium ion flow. This enhanced excitability reduces the voltage or the charge required to initiate an action potential. If charge is transferred efficiently between cells, either actively or passively, cell length is effectively multiplied in the linear model by the number of cells in the chain; this, in turn, reduces the external electric field required to generate a given voltage across a terminating membrane (see Chapter 11 in *BMA* by A. Pilla).

An interesting speculation that is raised by these adaptive processes is whether or not a neural network can be trained to identify a repetitive signal such as 60 Hz in the presence of larger electric fields generated by the surrounding biological material. To test this hypothesis, we programmed a computer to simulate a neural network as shown in Figure 5.12 [65]. Using a backpropagation algorithm to adjust the connecting weights between neurons, a sigmoidal summing junction to model the neurons, and a pseudorandom noise generator,

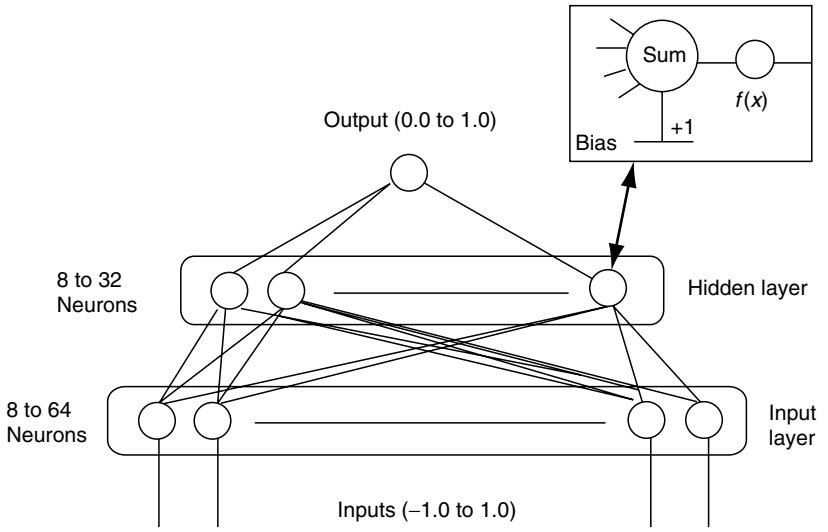

FIGURE 5.12
Backpropagation neural network. (From Barnes, F.S., *Bioelectromagn. Suppl.*, 1, 67–85, 1992. With permission.)

we measured the number of runs required to train the network to recognize a 60 Hz signal with 97% accuracy as a function of the input signal-to-noise ratio. The results in Figure 5.13 show that the training time increased from about 200 runs to about 1400 runs as the signal-to-noise ratio decreased from 1 to 0.001. The way the noise is presented to this network during the training makes a difference. For example, if you want the network to separate 59 Hz from 60 Hz, it helps to tell the network that 59 Hz is noise. This computer network model is clearly too simple to describe a biological nervous

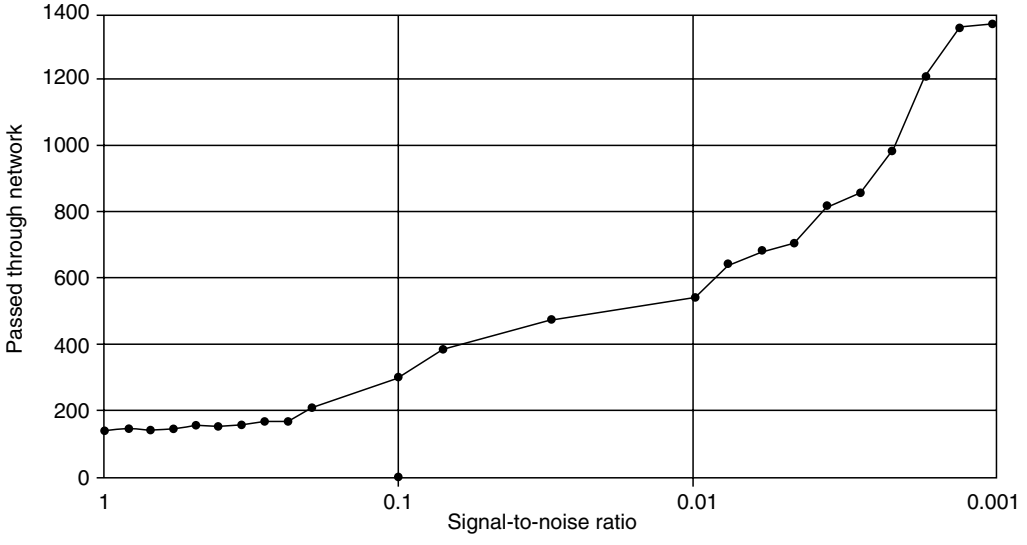

FIGURE 5.13
The learning response of a neural network with 64 input neurons, 8 neurons in the hidden layer, and 1 output neuron to a 60 Hz input signal and a pseudorandom noise signal with a decreasing signal-to-noise ratio. (From Barnes, F.S., *Bioelectromagn. Suppl.*, 1, 67–85, 1992. With permission.)

system, but it may provide a clue to one way in which a collection of cells may be able to respond to weak, externally applied electric fields, but a single cell would not.

5.7 Thermal Effects

One important effect of current flow due to electric fields is heating. The power input to a given volume of material can be expressed by $P' = I^2R$, where I is the total current and R is the resistance of the sample. For many calculations, a more useful expression is given by the power per unit volume or $P = \sigma E^2$, where σ is the conductivity, E is the electric field intensity. (For a more complete treatment of heating, see Chapter 10 and Chapter 12 of *BMA*.) The temperature rise resulting from this heat input is determined by the thermal capacity of the volume and the mechanisms for carrying the heat energy away. Typically, these thermal loss mechanisms include a combination of conduction and convection processes. For short current pulses, the heat dissipation is usually dominated by thermal conduction, and the basic equation for the rate of change of temperature is given by

$$\frac{\partial T}{\partial t} = \frac{P}{\rho' C_p} - \frac{T - T_0}{\tau_c} \tag{5.58}$$

where T is the temperature, T_0 is the initial temperature, t is time, and P is the power supplied per unit volume. ρ' is the density of the material (in kg/m^3), C_p is the specific heat under constant pressure, and τ_c is the thermal relaxation time.

If we consider a homogenous sphere of radius a immersed in an infinite fluid, the thermal conductive relaxation time is approximately given by

$$\tau_c = \frac{a^2}{4\overline{K}} \tag{5.59}$$

where $\overline{K}$ is the thermal diffusivity and is measured in meter square per second [84]. The thermal diffusivity is given by

$$\overline{K} = \frac{K'}{\rho' C_p} \tag{5.60}$$

where K' is the thermal conductivity (in cal/m sec °C), ρ' is the material density (in kg/m^3), and C_p is the thermal capacity (in cal/°C kg). If an applied current pulse is short compared to τ_c, the maximum temperature change is given by

$$\Delta T_{max} = \left(\frac{3}{2\pi e}\right)^{3/2} \frac{\overline{H}}{\rho' C_p a^3} \tag{5.61}$$

where $\overline{H}$ is the total input energy in calories and e is the base of natural logarithms [84]. For current inputs that are long compared to the thermal relaxation time τ_c, the peak temperature is determined by a balance between the input power and the dissipation process controlled by conduction and convection. It is interesting to note that if we assume the thermal properties of water as a first approximation to various kinds of tissue, then τ_c for a sphere with a equal to 1 μm is a little less than 2 μs. Since a sphere has the

smallest surface to volume ratio, Equation 5.60 gives an upper bound on τ_c, and Equation 5.61 gives an upper bound on the peak temperature excursion for small structures and pulses that are short compared to τ_c. Simply stated, it takes high power densities and large differential absorption coefficients to get significant differential temperature rises in small biological structures.

For situations where the volume involved is a cubic millimeter or larger, the thermal time constant is controlled by the amount of blood flowing through the volume. In these cases, temperatures may be more easily measured than calculated since a complicated thermal and electrical boundary value problem would have to be solved to calculate the temperature rise. This is particularly true since the viscosity η and other thermal and electrical parameters such as ρ, C_p, $\overline{K}$, etc. are functions of temperature. For example, C_p for an artificial bilipid membrane is shown in Figure 5.14 [85]. Another example of the importance of change in temperature is the conductivity of saline,

$$\sigma \approx C_1[10^{[(1/T)+\alpha](1/b)}] \times 10^{-4}\,\mathrm{S/m} \tag{5.62}$$

where C_1 is the concentration of NaCl in milligram equivalents per liter, T is the absolute temperature, $\alpha \simeq 6.23 \times 10^{-3}$ degrees^{-1}, and $b \simeq 1.4 \times 10^{-3}$ degrees^{-1} [86]. In the range around 37.5°C, this means that a 5°C change in temperature corresponds to a little less than 9% change in conductivity [86].

Changes in temperature are important, not only because they change transport properties such as viscosity, mobility, and the diffusion coefficient D, but also because they change chemical reaction rates. Typical biochemical reactions can be described by an equation of the form

$$\frac{dS}{dt} = -K'S \tag{5.63}$$

where S is the fraction of the material that has undergone the chemical reaction, t is the time, and K' is the reaction rate [87]. K' is often given by

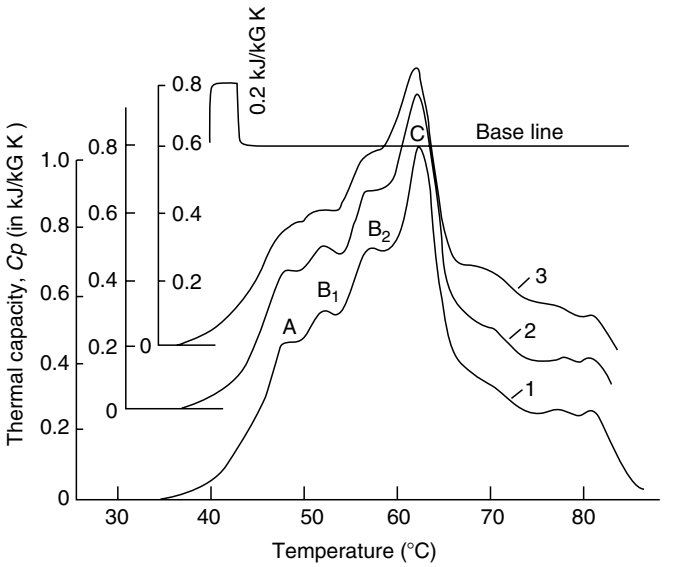

FIGURE 5.14
Differential changes in the heat capacity, C_p, of erythrocyte membranes as a function of temperature in 5 mmol/L sodium phosphate with pH 7.4 and a concentration of 5 mg protein per milliliter. The changes at A, B, B_2, and C correspond to changes in the structure of the membrane with temperature and are irreversible. Curve 1: intact membranes. Curve 2: irradiated at 330 mHz for 5 min (SAR 9 W/kg). Curve 3: irradiated at 300 mHz for 30 min (SAR W/kg). (From Shuyrou, V.L., Zhodan, G.G., and Akorv, I.G., Academy of Science, Institute of Biophysics, Pushchino, Moscow Region, Russia, personal communication, 1984. With permission.)

$$K' = \frac{kT}{h} \exp\left(\frac{+\Delta H' - T\Delta S'}{R'T}\right) \tag{5.64}$$

where k is the Boltzmann constant, T is the absolute temperature, H' is the free energy, S' is the entropy, h is Plank's constant, and R' is the gas constant. The significant feature is that the reaction rate K' varies exponentially with temperature, and $\Delta H'$ and $T\Delta S'$ are large numbers. Thus, very small changes in temperature can lead to big changes in chemical reaction rates.

In addition to chemical reaction rate changes, there may be changes in the binding of the proteins to cell membranes that lead to a shedding of proteins with a small increase in temperature. An exponential temperature dependence of the binding to membrane receptors is to be expected just as it is for chemical reactions [88].

A rule of thumb that the author uses to estimate whether or not significant biological changes are likely is to see if ΔT is $>10^{\circ}$C for 10^{-6} sec, 5°C for 1 sec, or 2°C for hours. If the ΔTs are larger, then they can be expected to lead to important changes in the biological system. Typical mammalian temperature regulatory systems will hold the internal body temperature constant to within $+/-0.5^{\circ}$C.

In addition to the magnitude of the temperature change, it can be shown that the rate of temperature rise, dT/dt, is important and can induce current to flow across membranes. Changes in the firing rate of pacemaker cells from the ganglion of *Aplysia* have been induced by total temperature changes of as little as $1/10^{\circ}$C when the rates of change are about 1°C/sec [89]. This change of the firing rate corresponds to the injection of approximately 1 nA into the cell. By taking the time derivative of the Nernst equation, which describes the passive equilibrium potential across a membrane for a single ion, it can be shown that a current proportional to the temperature derivative is to be expected, or

$$I = -qV_1'C_1\left(\frac{\phi}{\phi_T}\right)\left(\frac{\dot{\phi}}{\phi} - \frac{\dot{T}}{T}\right) \tag{5.65}$$

where q is the charge of the ion, V_1' is the volume of the cell, C_1 is the concentration of ions inside the cell, ϕ is the resting potential, ϕ is given by $\phi_T = \frac{kT}{q}$, $\dot{\phi}$ is the derivative of the membrane potential with respect to time, T is the temperature, and $\dot{T}$ is the temperature derivative with respect to time [90].

Bol'shakov and Alekseyev [91] have observed similar changes in the firing rate of pacemaker cells taken from the large parietal ganglion of the central nervous system of *Limnea stagnalis*. In their experiments they observed a slow increase in temperature (1°C/min or slower) to increase the firing rate of the pacemaker cell and a rapid increase in temperature (0.1°C/sec or faster) to decrease or stop the firing. They ascribe these changes to changes in the Na^+ pump as the rapid temperature effect was completely blocked by adding ouabain to the solution. In addition to the changes in the Na^+ currents, Ca^+ currents have been shown to be sensitive to rapid changes in temperature [92]. The rate of rise has also been shown to be significant in exciting a brain slice from a mouse with pulses of 10^{-3} sec and peak temperature rises of less than 0.5°C [93].

Temperature rises also lead to thermal expansion, and rapid temperature rises lead to the generation of acoustic waves [94]. These acoustic waves, in turn, can affect stretch receptors in nerve cells and other tissue and thus generate a biological response that may be at a considerable distance from the electrical heating [95].

To get an idea of the magnitudes of both heating (as described in Equation 5.58) and the effect of the rate of rise (as given by Equation 5.65), consider the case of liver tissue with $\sigma = 0.14$ S/m and a field strength in the tissue of 2×10^3 V/m. The rate of

temperature rise is approximately 13°C/sec assuming no conduction or convection heat losses and the thermal capacity of water. For this high field, a significant temperature rise occurs in about 1/2 sec. However, the rate of rise has been shown to be significant in exciting a brain slice from a mouse with pulses of 10^{-3} sec [96].

5.8 Natural Fields and Man-Made Fields

It is of interest to compare man-made with naturally occurring fields. First, we would like to know the approximate magnitudes of the fields that occur in nature outside man or the biological system of interest. Second, we would like to have values for the internal or physiological fields.

The natural electric fields at the surface of the earth have both DC and AC components [97]. One may think of the earth as a spherical capacitor where the surface is negatively charged with respect to an electrical conducting ionosphere that is about 50 km above the surface. This capacitor is being continuously charged by about 100 lightning strokes per second from thunderstorms worldwide. Since the atmosphere is a finite conductor, it also discharges with an *RC* time constant of about 18 sec. The result is an average electric field of about 130 V/m. This field is not uniform with height and typically falls off to 30 V/m at 1 km above the surface. The local values vary widely with temperature and humidity. In the Sahara during dust storms caused by winds in the dry season, a field of 1500 V/m has been measured with the polarity reversed from the normal. In thunderstorms, fields of up to 3000 V/m have been measured without lightning, and the polarity has been known to reverse in minutes. Storms as far as 50 km away have been shown to affect local fields. See Chapter 1 in this volume by Mild and Greenebaum for more details.

The atmosphere is a relatively poor conductor and as such will suspend a significant number of charged ions, dust particles, etc. This helps to contribute to local field variations of 20% to 50% over the course of the day and is a normal characteristic of our environment. The level of natural AC fields in the atmosphere falls very rapidly from a DC value of about 130 V/m [97]. The average value of the vertical component of the electric field above 1 Hz has a typical value of 10^{-4} V/m $\text{Hz}^{1/2}$. However, this value fluctuates widely with the time of day, the season of the year, and location. Additionally, the Schumann resonances impose multiple-cavity resonances on this spectrum with a periodicity of about 10 Hz. These resonances may be explained in terms of standing waves in a cavity formed by the earth and the atmosphere. These very low levels of the natural fields are one of the reasons why electronic communications in the ELF band are useful for ships at sea and submarines. However, because of the very low level of the natural atmospheric fields at frequencies above a few hertz, there is very little reason for biological organisms to develop natural protection against perturbations at these frequencies. It also means that biological systems could communicate internally at these frequencies using very low signal power levels and still maintain a good signal-to-noise ratio.

The signals generated within the body are the result of nerve firing and other cell activity. A typical nerve cell fires with an action potential of 50 to 100 mV and transmits a current pulse about 0.4 ms long [98]. The rise time for this current spike is approximately 0.1 ms, and the fall time is about 0.5 ms. Each pulse is followed by a refractory period that is typically on the order of 1 to 3 ms. The longitudinal fields along the exterior of a nerve cell membrane are estimated to have a maximum value of about 5×10^{-2} V/m during an action potential when the cell is surrounded by a relatively high conductivity fluid of 5 S/

m [98]. If we look at these signals closely, it will be noted that the interspike interval along any given nerve cell fluctuates in time. Additionally, variations in the beat-to-beat intervals for the ECG are random or chaotic, and the period can vary up to 30%. This is frequently seen, particularly at slow heart rates.

In looking at the natural fields in the body, we have two concerns. The first is how large an external signal takes to perturb the ongoing natural signal that is being used to communicate or control some biological process [99]. The second is how much of the signal field typically leaks away from active nerve fibers or bundles to form a background noise environment for surrounding tissue and processes. Regarding the first of these questions, it is interesting to look on the microscopic level at the electrical noise, i.e., the fluctuations that occur fundamentally as a result of the electrical process itself.

The first of several sources of noise that are always present is blackbody radiation, or Johnson noise, which is given by

$$P_{\mathrm{n}} = kTB \tag{5.66}$$

where P_{n} is the noise power, k is the Boltzmann constant, T is the absolute temperature, and B is the bandwidth [100–102]. The voltage equivalent of this noise power, which can be delivered to a matched load, or the mean squared voltage fluctuation $\overline{V}_{\mathrm{n}}{}^2$ across a resistance R, is given by [101,102]

$$\overline{V}_{\mathrm{n}}^2 = 4kTBR \tag{5.67}$$

or by the mean squared current fluctuations

$$\bar{i}_{\mathrm{n}}^2 = \frac{4kTB}{R} \tag{5.68}$$

Johnson noise applies to systems at thermodynamic equilibrium. Living systems are not at thermodynamic equilibrium. Thus, the foregoing expressions must be applied with caution to only those portions of biological systems where thermodynamic equilibrium is a good approximation. In the case of lasers, the spontaneous emission noise associated with the nonequilibrium population inversion of the energy levels can be obtained from Planck's radiation law by defining a negative temperature that assumes a Boltzmann distribution of atoms with N_2 atoms in the excited energy level E_2, which is greater than the N_1 atoms in the energy level E_1, such that

$$\frac{N_1}{N_2} = \exp\left[\frac{E_2 - E_1}{kT}\right] \tag{5.69}$$

In this case, the spontaneous emission noise $P_{\mathrm{n}} = h\upsilon B$, where h is Planck's constant and υ is the frequency of the radiation corresponding to a transition from E_2 to E_1 [100]. In those situations where the nonequilibrium characteristic may be described by an amplifier that can be modeled by a negative resistor or by energy storage in an inverted population distribution, the concept of a negative temperature may be a useful approach. Note that an equivalent temperature, T, is a convenient way to describe the energy distribution of a large number of particles. A much more complete description of nonequilibrium noise is given in Chapter 7 in this volume.

The second source of noise that is also present is the shot noise, which is given by

$$\bar{i}_{\mathrm{n}}^2 = 2q\bar{I}_{\mathrm{DC}}B \tag{5.70}$$

where $\bar{i}_n^2$ is the mean-squared current fluctuation. This noise comes about because of the discreteness of the electronic charge q and the assumption that the motion of each charge is independent. With negative feedback, this noise may be reduced, as has been shown for space charge-limited diodes. Shot noise results in an AC fluctuation, $\bar{i}_n^2$, which is proportional to the average value of the current, $\bar{I}_{DC}$. A third source of noise is $(1/f)$ noise. This noise may be generated by many processes, some of which are described in Chapter 7 in this volume. $1/f$ noise can be synthesized from Gaussian noise by filtering it with a circuit that requires about one low pass state variable per decade for the period of time over which the model is used to generate noise with a power density spectrum $S(f) = (C/f^{\alpha})$, where C is a constant and α is a constant between 1 and 2 [103]. We can expect to find this kind of noise for processes that evolve with time and, or have memory. $1/f$ noise describes the power spectral density of the fluctuations at low-frequencies in such diverse phenomena as transistors, quartz crystal oscillators, the closing Dow Jones Averages for the stock market, and the weather. It is also generated by the flow of ion currents through an orifice and thus is a fundamental part of the transport of current through channels in membranes [102]. Measurements of the noise voltage across a 10 μm hole in a 6 μm Mylar film showed that for a wide range of ionic concentrations the voltage noise spectral density $S(f)$ is given by

$$\frac{S_\phi(f)}{\phi^2} = \frac{a}{bnr^3 f} \tag{5.71}$$

where b is a numerical geometric factor, n is the density of ions in the solution, r is the radius of the hole, a is a constant, and ϕ is the applied voltage. The data showed that $2.5 < a < 40$ with a mean value of 10 for a wide range of solutions including HCl, KCl, and AgNO, with concentrations from 0.05 to 5 mol.

For natural membranes, this noise has been shown to take the form of

$$S_E(f) = \frac{C_E}{f^{\alpha}} \tag{5.72}$$

where $0.7 < \alpha < 1.2$ with a mean close to $\alpha = 1$. For the frog node of Ranvier, the noise is a function of the membrane voltage as shown in Figure 5.15 [104]. The dominant source of this noise appears to be the K^+ current, and it has a minimum when the membrane is biased, so that this K^+ current is biased to zero.

To get an estimate of the size of these noise sources, let us consider a pacemaker cell from the abdominal ganglion of *Aplysia*. This cell fires 20-ms pulses at about 1 Hz/sec. It has a resting voltage of about 50 mV and a resistance R measured with a microelectrode between the inside of the cell and the surrounding solution of approximately 10^6 Ω. If we assume a system bandwidth of 100 Hz and $T = 300$ K, the Johnson noise voltage would be $\overline{V}_n \approx 3 \times 10^{-6}$ V. This gives a resting potential-to-noise ($\overline{V}_n$) ratio of about 4×10^4. The peak current flow in these cells is estimated to be about 10^{-7} A, and thus the estimated shot noise current is $\bar{i}_n \approx 2 \times 10^{-12}$ A, and the ratio of the peak current to the noise current is about 2×10^4. We do not have the available value $S(f)$ for the *Aplysia*, $\bar{v}_\phi = \sqrt{S(f)B}$, where B is the bandwidth. If it is assumed that the maximum value of the noise is the same as that of the frog node of Ranvier, then for a bandwidth of 1 Hz we get $\bar{v}_\phi = 1.4 \times 10^{-5}$ V at a center frequency of 1 Hz from the curve for −50 mV in Figure 5.15. This is about a factor of 10^3 greater than the Johnson noise. It is likely that $(1/f)$ noise is the largest source of noise at the cell membranes for frequencies below 160 Hz [105,106].

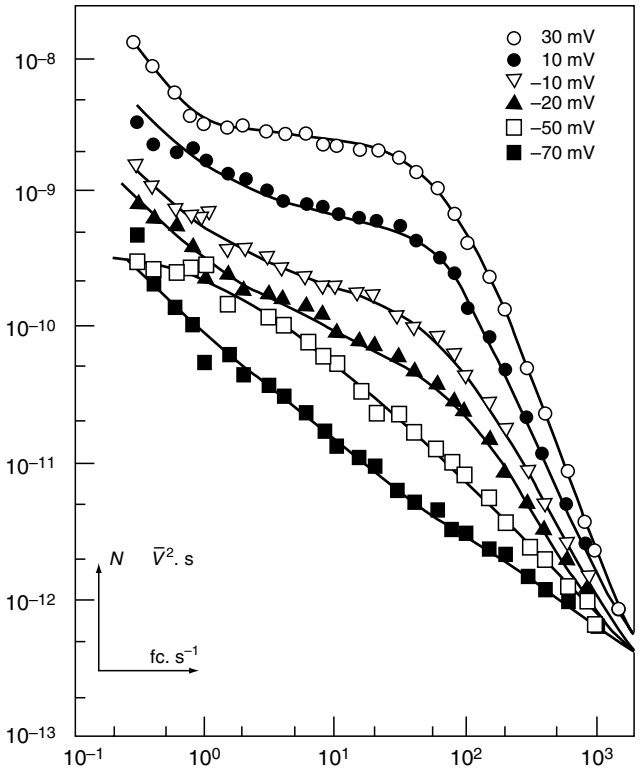

FIGURE 5.15
Voltage noise spectra of a frog node of Ranvier at different levels of membrane potential. (From Sichenga, E. and Verveen, A.A., in *Proceedings of the 1st European Biophysics Congress*, Vol. 5, Verlag Wiener Medizinischen Akademic, Vienna, Austria, 219, 1971. With permission.)

These fundamental sources of noise, which are generated by random fluctuations in the position of ions and their transport through channels, are spatially incoherent [73]. For many processes the important quantity in deciding whether or not an electrical signal is biologically important is the signal-to-noise ratio S/N where S is the power in the signal and N is the noise power. Typically, it is assumed that a signal-to-noise ratio of 1 is required for an externally applied signal to be detectable. In the foregoing discussion for both thermal and shot noise the movement of each charge was assumed to be statistically independent of each other. If for an externally applied signal the openings of the channels in a cell are excited in parallel and coherently and the noise is generated by incoherent random firing, then the signal-to-noise ratio increases with the square root of the number of channels. Similarly, the signal-to-noise ratio for a bundle of nerves would be expected to increase with the square root of the number of nerves for a signal applied externally to the whole bundle. Thus, a collection of cells can be expected to detect smaller signals than a single cell.

In addition to the electrical noise generated by currents and voltages that are part of the single-cell operation, electrical signals propagate through the body as a result of the incomplete confinement of electrical signals propagating in nerve cells. In a sense, these signals may be thought of as noise if they are not pertinent to the activity in that portion of the body through which they are propagating. If, on the other hand, they are used by tissue within the organism at some distance from the source, they must be thought of as signals. In the brain, the fraction of these signals that reach the scalp is called the electroencephalogram (EEG). The EEG is obtained by placing two or more conducting electrodes on the scalp and measuring the voltage between them. For electrodes placed 5 cm apart, the peak-to-peak voltages range up to 30 μV [107]. The author views this voltage as the integral of the vector sum of the leakage fields from the firing of the nerve

cells in the brain between the two electrodes. Since there are a very large number of cells firing, most of the 50 mV signals from an isolated nerve are canceled by summing over many like cells firing at different times and by the attenuation caused by propagation through the tissue. Estimates of surface potential gradients along a nerve fiber range from 3×10^{-4} to 5×10^{-2} V/m, and the corresponding current densities external to the nerve cells range from 5×10^{-2} to 4 A/m^2 [107,108]. The EEG voltage has a strong periodic component (particularly during sleep) near 10 Hz, which is known as the alpha (α) wave. A peak amplitude of this component may be as large as 50 μV when measured at the surface of the scalp. It is interesting to note that the EEG signal contains significant information on the brain's activity, and a few individuals have been trained to control these signals so as to control a computer in way that allows them write messages.

At the surface of the chest, a signal may be recorded between two electrodes known as the ECG or EKG (electrocardiogram). This signal results from the highly coordinated firing of the cells in the heart and has a definite wave shape that is closely related to the operation of the heart. The peaks of the so-called R wave in this signal may range up to 2.5 mV and are typically 0.5 to 1.5 mV, depending on the placement of the electrodes, the amount of body fat, etc. The pulse repetition rate is usually in the range of 1 to 2 Hz, and the ''QRS spike'' of the typical cardiogram is 40 ms long. Again, the signal measured at the surface of the skin is the result of leakage from electrically active cells located at a distance. The estimated current density near the firing heart cell ranges up to 1 A/m^2 [109]. In this case the shape of the signal reaching the skin is so closely related to the activity of the heart that it provides detailed information on heart function.

One result of electric discharges in the atmosphere, as well as natural ionizing radiation, is the creation of small positive and negative ions in the atmosphere. In clean country or mountain air, the typical ion density is about 10^{10}/m^3 with an average ion lifetime of a few minutes [110]. When a hot dry wind is blowing, positive ions created by the shearing forces can increase in concentration significantly. It has been shown that increases in the negative ion concentration reduce the amount of serotonin (5-HT) in mice and rabbits, possibly by accelerating the enzymatic oxidation process [111]. A similar result has been demonstrated in the oxidation of cytochrome *c*. Positive ions appear to block monoamine oxidase action, thus raising the concentration of free 5-HT [111]. Changes in 5-HT levels produce significant changes in the central nervous system, with high levels of positive ions raising the anxiety levels under stress. Other effects of increased positive ion concentration include a decrease in the survival rate of mice exposed to a measured dose of influenza virus, while an increase of negative ions reduced the mortality rate [111].

The significance of these results is that it is relatively easy to change the ion concentration in air using high-voltage DC systems where a leakage current of 1 μA from a burr or other sharp point would correspond to the generation of about 10^{12} ions per second.

Relatively few high-voltage DC transmission lines are in use today for distribution of power. Because the shocks resulting from a short contact across a high DC voltage are so painful and obviously dangerous, these systems are nearly always shielded. Thus, one is rarely exposed to DC electric fields $>10^3$ V/m. An additional feature of this exposure is that air is such a good insulator that the DC currents flowing through the body in a noncontacting situation are very small, as explained in the Introduction. For example, 1000 V across a 1-cm gap would yield a current density of approximately 10^{-7} A/m^2 flowing across the air gap. Thus, the principal hazards from DC fields occur when parts of the body make contact with a conductor.

5.9 Discussion and Summary

In this review some of the physical mechanisms by which DC and time-varying electric fields affect biological systems are presented. A few typical values of electric field strengths and current densities that are known to affect the biological system are compared with those of natural fields and other forces. Some values of electric fields and their gradients that are shown to modify the currents and shift energy levels are given. These in turn are shown to modify chemical reaction rates, which can lead to changes in the growth cells and other characteristics of biological systems. It is hoped that this information will help the readers to make their own estimates of when a given exposure to electric fields will be significant in modifying biological systems and provide a basis for understanding some of the biological results presented in other chapters of this handbook.

Acknowledgments

The author wishes to express appreciation to Mikhail Zhadin, Howard Wachtel, Maria Stuchly, Ross Adey, Mike Marron, Elliot Postow, Charles Polk, and many students for their many helpful comments and suggestions and to Adam Sadoff for help in the preparation of the text. He also wishes to express his appreciation to the Office of Naval Research under Contract N000l4-81-K-0387, the Mobile Manufactures Form, and the University of Colorado for financial support of his work in this area.

References

1. Yariv, A., *Optical Electronics in Modern Communications*, 5th edition, Oxford University Press, Oxford, UK, 1997.
2. Barnes, F.S. and Hu, C.L., Nonlinear interacations of electromagnetic waves with the biological materials, in *Nonlinear Electromagnetics*, Uslenghi, P.L.L., Ed., Academic Press, New York, 391–426, 1980.
3. Singer, S.J. and Nicolson, G.L, The fluid mosaic model of the structure of cell membranes, *Science*, 175, 720–731, 1972.
4. Poo, M., *In situ* electrophoresis or membrane components, in *Annual Review of Biophysics and Bioengineering*, Vol. 10, Mullins, L.J., Ed., Academic Press, New York, 245–276, 1981.
5. Kyriacous, D., *Modern Electroorganic Chemistry*, Springer-Verlag, Berlin, 1994.
6. Pohl, H.A., Dielectrophoresis, the behavior of neutral matter, in *Nonuniform Electric Fields*, Cambridge University Press, Cambridge, MA, 1978.
7. Kwon, Y. and Barnes, F.S., A theoretical study of the effects of RF fields in the vicinity of membranes, *Bioelectromagnetics*, 26, 2, 118–124, 2005.
8. Bier, M., Ed., *Electrophoresis: Theory, Methods, and Applications*, Vol. 2, Academic Press, New York, 1967.
9. Gascoyne, P.R. and Vykoukal, J.V., Dielectrophoresis-based sample handling in general-purpose programmable diagnostic instruments, *Proc. IEEE*, 92, 1, 22–41, 2004.
10. Rand, E.P., Interacting phospholipids bilayers: measured forces and induced structural changes, in *Annual Review of Biophysics and Bioengineering*, Vol. 10, Mullins, L.J., Ed., Academic Press, New York, 277–314, 1981.

11. Pethig, R., *Dielectric and Electronic Properties of Biological Materials*, John Wiley & Sons, New York, 184, 1979.
12. Parsegian, J.L., Long range physical forces in the biological milieu, in *Annual Review of Biophysics and Bioengineering*, Mullins, L.J., Ed., Academic Press, New York, 1973, 221.
13. Lifshitz, F.M., *Zh. Eksp. Teor. Fiz*., 29, 95, 1955; *Sov. Phys. JETP* 2, 73, 1956.
14. Iralelachvili, J., *Intermolecular and Surface Forces*, 2nd edition, Academic Press, San Diego, CA, 1992.
15. Tasao, Y.T., Evan, D.F., and Wennerstrom, H., Long-range attractive force between hydrophobic surfaces observed by atomic force microscopy, *Science*, 262, 1993.
16. Barnes, F.S., Ginley, H., and Shulls, W., AC electric field effects on bacteria, presented at the Third Annual Conference, Bioelectromagnetics Society (BEMS), Washington, DC, 1981.
17. Zumdahl, S.S., *Chemistry*, 2nd edition, D.C. Health Co., Lexington, MA, 546, 1989.
18. Atkins, P.W., *Physical Chemistry*, 4th edition, W.H. Freeman Co., New York, Chapter 26, 1990.
19. McCaig, C.D., Spinal neurite reabsorption and regrowth *in vitro* depend on the polarity of an applied electric field, *Development*, 100, 31–41, 1987.
20. Nuccitelli, R., Physiological electric fields can influence cell motility, growth, and polarity, *Adv. Cell Biol*., 2, 213–233, 1988.
21. Erickson, C.A. and Nuccitelli, R., Embryonic fibroblast motility and orientation can be influenced by physiological electric fields, *J. Cell Biol*., 98, 296–307, 1984.
22. Seto, Y.J. and Hsieh, S.T., Electromagnetic induced kinetic effects on charged substrates in localized enzyme systems, *Biotechnology and Bioengineering*, XVIII, 813–837, 1976.
23. Muraji, M., Nishimura, M., Tatebe, W., and Fujii, T., Effect of alternating magnetic field on the growth of the primary root of corn, *IEEE Trans. Magn*., 28, 4, 1996–2000, 1992.
24. Towns, C. and Schawlow, A., *Microwave Spectroscopy*, McGraw-Hill, New York, 255–283, 1955.
25. Bublitz, G.U. and Boxer, S.G., Stark spectroscopy: applications in chemistry, biology, and materials science, *Ann. Rev. Phys. Chem*., 48, 213–242, 1997.
26. Steiner, U. and Ulrich, T., Magnetic field effects in chemical kinetics and related phenomena, *Chem. Rev*., 89, 47–151, 1989.
27. Guyton, A.C., *Textbook of Medical Physiology*, 8th edition, W.B. Saunders, Philadelphia, PA, 47, 1991.
28. Barnes, F., A model for the detection of weak ELF electric and magnetic fields, *Bioelectrochem. Bioenerg*., 47, 207–212, 1999.
29. Alkon, D. and Rasmussen, H., A spatial-temporal model of cell activation, *Science*, 26, 998–1004, 1989.
30. Louisell, W., *Coupled Mode and Parametric Electronics*, John Wiley & Sons, New York, 1960.
31. Moss, F., Stochastic resonance, *Ber. Bunsenges. Phys. Chem*., 95, 3, 302–311, 1991.
32. Gammaitoni, L., Stochastic resonance, *Rev. Mod. Phys*., 70, 1, 223–287, 1998.
33. McNamara, B. and Wiesenfeld, K., Theory of stochastic resonance, *Phys. Rev. A*, 39, 9, 4854–4869, 1989.
34. MacGregor, R.J. and Lewis, E.R., *Neural Modelling*, Plenum Press, New York, 1977.
35. Cooper, M.S., Miller, J.P., and Fraser, S.E., Electropheretic repatterning of charged cytoplasmic molecules within tissues coupled by gap junctions by externally applied electric fields, *Dev. Biol*., 132, 170–188, 1989.
36. Epstein, B.R. and Foster, K.R., Anisotropy in the dielectric properties of skeletal muscle, *Med. Biol. Eng. Compnt*., 21, 51, 1983.
37. Kalmijn, A.J., Electric and magnetic field detection in elamobranch fishes, *Science*, 281, 916–918, 1982.
38. Kalmijn, A.J., Detection of weak electric fields, in *Sensory Biology of Aquatic Animals*, Atema, E.J. et al., Eds., Springer-Verlag, Berlin, Chapter 6, 1987.
39. McCleave, J.D, Rommel, S., and Cathcart, A.S., Weak electric and magnetic fields in fish orientation, in *Orientation: Sensory Basis*, Vol. 188, Adler, H.E., Ed., New York Academy of Sciences, New York, 270, 1971.
40. Ransom, B.P. and Eyring, H., Membrane permeability and electrical potential, in *Ion Transport across Membranes*, Clarke, H.J. and Nachmansohn, D., Eds., Academic Press, New York, 103, 1954.

41. Tsong, T.Y., Liu, D.S., and Chauvin, R., Electroconformational coupling (ECC): an electric field induced enzyme oscillation for cellular energy and signal transductions, *Bioelectrochem. Bioenerg.*, 21, 319–331, 1989 (a section of *J. Electroanal. Chem.* and constituting Vol. 275, Elsevier Sequoia, S.A., Lausanne, Switzerland, 1985).
42. Liu, D.S., Astumian, R.D., and Tsong, T.Y., Activation of Na^+ and K^+ pumping modes of (Na, K)-ATPase by an oscillating electric field, *J. Biol. Chem.*, 265, 13, 7260–7267, 1990.
43. Horn, L.W., A novel method of the observation of membrane transporter dynamics, *Biophys. J.*, 64, 281–289, 1993.
44. Triffet, T. and Green, H.S., Information and energy flow in a simple nervous system, *J. Theor. Biol.*, 86, 3, 1980.
45. Vaccaro, S.R. and Green, H.S., Ionic processes in excitable membranes, *J. Theor. Biol.*, 81, 771, 1979.
46. Eckert, R. and Ewald, D., Residual calcium ions depress activation of calcium-dependent current, *Science*, 216, 730, 1982.
47. Baumann, G. and Easton, G., Modeling state-dependent sodium conductance data by memoryless random process, *Math. Biosci.*, 60, 265, 1982.
48. Schauf, C.L. and Baumann, G., Experimental evidence consistent with aggregation kinetics in sodium current of myxicola giant axons, *Biophys. J.*, 35, 707, 1981.
49. Baumann, G. and Eastman. G.S., Charge immobilization linked to inactivation in the aggregation model of channel gating, *J. Theor. Biol.*, 99, 249, 1982.
50. Poo, M., Rapid lateral diffusion of functional ACh receptors in embryonic muscle cell membrane, *Nature*, 295, 332, 1982.
51. Poo, M. and Lam, J.W., Lateral electrophoresis and diffusion of concanavalin A receptors in the membrane of embryonic muscle cell, *J. Cell Biol.*, 76, 483, 1978.
52. Lee, K.Y.C., Lingler, J.B., and McConnnell, H.M., Electric field-induced concentration gradients in lipid monolayers, *Science*, 263, 655, 1994.
53. Hayashi, H. and Fishman, H., Inward rectifier K^+ channel from analysis of the complex conductance of aplysia neuronal membrane, *Biophys. J.*, 53, 747–757, 1988.
54. Barnes, F.S. and Hu, C.L., Model for some non thermal effects of radio and microwave fields on biological membranes, *IEEE Trans. Microwave Theory Technol.*, 25, 742, 1977.
55. Montaigne, K. and Pickard, W.F., Offset of the vascular potential of characean cells in response to electromagnetic radiation over the range of 250 Hz to 250 kHz, *Bioelectromagnetics*, 5, 31, 1984.
56. Pickard, W.F. and Rosenbaum, F.J., Biological effects of microwaves at membrane level: two possible athermal electrophysiological mechanisms and a proposed experimental test, *Math. Biosci.*, 39, 235, 1978.
57. Pickard, W.F. and Barsoum, Y.H., Radio-frequency bioeffects at the membrane level: separation of thermal and athermal contributions in the Characeae, *J. Membrane Biol.*, 61, 39, 1981.
58. Kalkwarf, D.R., Frasco, D.L., and Brattain, W.H., Current rectification and action potentials across thin lipid membranes, in *Physical Principles of Biological Membranes*, Snell, F., Wolken, J., Iverson, G., and Lam, J., Eds., Gordon & Breach, New York, 1970.
59. Franceschetti, G. and Pinto, I., Cell membrane nonlinear response to applied electromagnetic field, *IEEE Trans. Microwave Theory Technol.*, 32, 7, 1984.
60. Casaleggio, A., Marconi, L., Morgavi, G., Ridella, S., and Rolando, C., Current flow in a cell, with a nonlinear membrane, stimulated by an electric field, personal communication, 1985.
61. Cain, C.A., Biological effects of oscillating electric fields: role of voltage sensitive ion channels, *Bioelectromagnetics*, 2, 23, 1981.
62. Bisceglia and Pinto, I., Volterra series solution of Hodgkin–Huxley equation, personal communication, 1984.
63. Wachtel, H., Firing-pattern changes and transmembrane currents produced by low frequency fields in pacemaker neurons, in *Proceedings of the 18th Annual Hansford Life Science Symposium*, Technical Information Center, U.S. Department of Energy, Richland, WA, 132–147, 1978.
64. Adler, R., A study of locking phenomena in oscillators, *Proc., IEEE* 34, 351, 1946.
65. Barnes, F.S., Smoller, A., and Sheppard, A., Injection locking of pacemaker cells, in *Proceedings of the 9th Annual Conference*, IEEE Engineering in Medicine and Biology Society, 1986.

66. Fohlmeister, J.F., Adelman, W.J., Jr., and Poppele, R.E., Excitation properties of the squid axon membrane and model systems with current stimulation, *Biophys. J.*, 30, 79–98.
67. Barnes, F.S., Some engineering models for interactions of electric and magnetic fields with biological systems, *Bioelectromagn. Suppl.*, 1, 67–85, 1992.
68. Kroupa., V.F., *Frequency Synthesis*, John Wiley & Sons, New York, 1973.
69. Koss, D.A. and Carstensen, E. L, Effects of ELF electric fields on the isolated frog heart, *IEEE Trans. Biomed. Eng.*, 30, 347, 1983.
70. Litovitz, T.A., Krause, D., and Mullins, J.M., Effect of coherence time of the applied magnetic field on ornithine decarboxylase activity, *Biochem. Biophys. Res. Commun*, 178, 3, 862–865, 1991.
71. Mullins, J.M., Krause, D., and Litovitz, T.A., Simultaneous application of a spatially coherent noise field blocks use response of cell cultures to a 60 Hz electromagnetic field, in *Proceedings of the 1992 World Congress on Bioelectromagnetism*, Bioelectroemagnetics Society, Orlando, FL, 1992.
72. Farrell, J.M., Barber, M., Krause, D., and Litovitz, T.A., The superposition of a temporally incoherent magnetic field inhibits 60 Hz-induced changes in the ODC activity of developing chick embryos, *Bioelectromagnetics*, 19, 53–56, 1998.
73. Litovitz, T.A., Montrose, C.J., Doinov, P., Brown, K.M., and Barber, M., Superimposing spatially coherent electromagnetic noise inhibits field induced abnormalities in developing chick embryos, *Bioelectromagnetics*, 15, 2, 105–113, 1994.
74. Walleczek, J. and Liburdy, R.P., Nonthermal 60 Hz sinusoidal magnetic-field exposure enhances $^{45}Ca^{2+}$ uptake in rat hymocytes: dependence on mitogen activation, *Fed. Eur. Biochem. Soc. Lett.*, 271, 1/2, 157–160, 1990.
75. Liburdy, R.P., Calcium signaling in lymphocytes and ELF fields, *Fed. Eur. Biochem. Soc.*, 301, 1, 53–59, 1992.
76. Liburdy, R.P., Biological interactions of cellular systems with time-varying magnetic fields, *Ann. N.Y. Acad. Sci.*, 649, 74–94, 1992.
77. Yost, M.G. and Liburdy, R.P., Time-varying and static magnetic fields act in combination to alter calcium signal transduction in the lymphocyte. *Fed. Eur. Biochem. Soc.*, 296, 2, 17–122, 1992.
78. McLeod, K, J., Lee, R.C., and Ehrlich, H.P., Frequency dependence of electric field modulation of fibroblast protein synthesis, *Science*, 136, 1465–1469, 1987.
79. Takashima, S., Non-linear properties of nerve membranes, *Biophys. Chem.*, 11, 447, 1980.
80. Berkowitz, G.C. and Barnes, F.S., The effects of nonlinear membrane capacity on the interaction of microwave and radio frequencies with biological materials, *IEEE Trans. Microwave Theory Technol.*, 27, 204, 1979.
81. Alkon, D.L., Memory storage and neural systems, *Sci. Am.*, 261, 42–50, 1989.
82. Alkon, D.L. and Rasmussen, H., A spatial temporal model of cell activation, *Science*, 26, 998–1004, 1988.
83. Yang, X., Korn, H., and Faver, A.S., Long-term potentiation of electronic coupling at mixed synapses, *Nature*, 348, 542–545, 1990.
84. Hu, C.L. and Barnes, F.S., The thermal chemical damage in biological materials under laser irradiation, *IEEE Trans. Biomed. Eng.*, 17, 220, 1970.
85. Shuyrou, V.L., Zhodan, G.G., and Akorv, I.G., Effects of 330 MHz radio frequency, Academy of Science, Institute of Biophysics, Pushchino, Moscow Region, Russia, personal communication, 1984.
86. Trautman, E.D. and Newbower, R.S., A practical analysis of the electrical conductivity of blood, *IEEE Trans. Biomed. Eng.*, 30, 141, 1983.
87. Johnson, F. H, Eyring, H., and Stover, B.J., *The Theory of Rate Processes in Biology and Medicine*, John Wiley & Sons, New York, 1974.
88. Liburdy, R.P. and Penn, A., Microwave bioeffect in erythrocyte are temperature and pO dependent action permeability and protein shedding occur at the membrane phase transition, *Bioelectromagnetics*, 5, 283–291, 1984.
89. Chalker, R., The effect of microwave absorption and associated temperature dynamics on nerve cell activity in Aplysia, M.S. thesis, University of Colorado, Boulder, 1982.
90. Barnes, F.S., Cell membrane temperature rate sensitivity predicted from the Nernst equation, *J. Bioelectromagn.*, 5, 113, 1964.

91. Bol'shakov, M.A. and Alekseyev, S.I., Change in the electrical activity of the pacemaker neurons of *L. stagnalis* with the rate of their heating, *Biophysics*, 31, 569–571, 1986.
92. Alekseyev, S.I., IL'in, V.I., and Tyazhelov, V.V., Effect of electromagnetic radiation in decimeter wavelength range on calcium current of mollusk neurons, *Biophysics*, 31, 2, 290–295, 1986.
93. Philippova, T.M., Novoselov, V.I., Bystrova., M.F., and Alekseev, S.I., Microwave effect on camphor binding to rat olfactory epithelium, *Bioelectromagnetics*, 9, 347–354, 1988.
94. Bushanam, S. and Barnes, F.S., Laser generated thermoelastic shock waves in liquids, *J. Appl. Phys*., 46, 5, 2074–2082, 1975.
95. Mihran, R.T., Barnes, F.S., and Wachtel, H., Temporally-specific modification of myelinated axon excitability *in vitro* following a single ultrasound pulse, *Ultrasound Med. Biol*., 16, 3, 297–309, 1990.
96. Ady, G., McNaughton, B.L., and Wachtel, H., A system for recording microwave effects on isolated mammalian brain slices, presented at the 5th Annual Conference, Bioelectromagnetics Society, Boulder, CO, 1983.
97. Polk, C., Sources, propagation amplitude and temporal variations of extremely low frequency (0–100 Hz) electromagnetic fields, in *Biological and Clinical Effects of Low-Frequency Magnetic and Electric Fields*, Llaurado, J.G., Sances, A., Jr., and Battocletti, J.H., Eds., Charles C Thomas, Springfield, IL, 21, 1974.
98. Plonsey, R., *Bioelectric Phenomena*, McGraw-Hill, New York, 1969.
99. Barnes, F.S. and Seyed-Madani, M., Some possible limits on the minimum electrical signals of biological significance, in *Mechanistic Approaches to Interactions of Electric and Electromagnetic Fields with Living Systems*, Blank, M. and Findl, E., Eds., Plenum Press, New York, 339–349, 1987.
100. Yariv, A, *Introduction to Optical Electronics*, Holt, Reinhart & Winston, New York, 1976.
101. MacDonald, D.K.C., *Noise and Fluctuations: An Introduction*, John Wiley & Sons, New York, 1962.
102. Beck, A.H.W., *Statistical Mechanics, Fluctuations, and Noise*, Edward Arnold, London, 1967.
103. Keshner, M.F., 1/f noise, *Proc. IEEE*, 70, 3, 212–218, 1982.
104. Sichenga, E. and Verveen, A.A., The dependence of the 1/f noise intensity of the diode of Ranvier on membrane potential, in *Proceedings of the 1st European Biophysics Congress*, Vol. 5, Verlag Wiener Medizinischen Akademic, Vienna, Austria, 219, 1971.
105. Dorset, D.L. and Fishman, H.M., Excess electrical noise during current flow through porous membranes separating ionic solutions, *J. Membrane Biol*., 21, 291–301, 1975.
106. Verveen, A.A. and DeFelice, L.J., Membrane noise, *Prog. Biophys. Mol. Biol*., 28, 189, 1974.
107. Nuney, P.L. and Katznelson, R. D., *Electric Fields of the Brain—The Neurosphysics of EEG*, Oxford University Press, New York, 1981.
108. Bernhardt, J., The direct influence of electromagnetic fields on nerve and muscle cells of man within the frequency range of 1 Hz to 30 MHz, *Radiat. Envriron. Biophys*., 16, 309, 1979.
109. Verveen, A.A. and Derksen, H.E., Fluctuation phenomena in nerve membrane, *Proc. IEEE*, 56, 906, 1968.
110. Beckwith, J.R. and McGuire, L.B., *Basic Electrocardiography and Vector Cardiography*, Raven Press, New York, 1982.
111. Krueger, A. and Reed, E., Biological impact of small air ions, *Science*, 193, 1209, 1976.
112. Weaver, J. C. and Chizmadzhev, Y., Electroporation, *Biological and Medical Aspects*, Barnes, F.S. and Greenebaum, B., Eds., Taylor & Francis, Boca Raton, FL, Chapter 9, 2006.
113. Michaelson, S.M., Elson, E.C., Anderson, L.E., Interaction of non-modulated and pulse modulated radio frequency fields with living fields with living matter: experimental results, *Biological and Medical Aspects*, Barnes, F.S., and Greenebaum, B., Eds., Taylor & Francis, Boca Raton, FL, Chapter 3, 2006.
114. Pilla, A.A., Mechanisms and therapuetic applications of time-varying and static magnetic fields, *Biological and Medical Aspects*, Barnes, F.S., and Greenebaum, B., Eds., Taylor & Francis, Boca Raton, FL, Chapter 11, 2006.